Review Article

Curved carbon nanotubes: From unique geometries to novel properties and peculiar applications

Lizhao Liu[1,2], Feng Liu[2] (✉), and Jijun Zhao[1] (✉)

[1] *Key Laboratory of Materials Modification by Laser, Ion and Electron Beams (Dalian University of Technology), Ministry of Education, Dalian 116024, China*
[2] *Department of Materials Science and Engineering, University of Utah, Salt Lake City, Utah 84112, USA*

ABSTRACT

Incorporating pentagons and heptagons into the hexagonal networks of pristine carbon nanotubes (CNTs) can form various CNT-based nanostructures, as pentagons and heptagons will bend or twist the CNTs by introducing positive and negative curvature, respectively. Some typical so-made CNT-based nanostructures are reviewed in this article, including zero-dimensional toroidal CNTs, and one-dimensional kinked and coiled CNTs. Due to the presence of non-hexagonal rings and curved geometries, such nanostructures possess rather different structural, physical and chemical properties from their pristine CNT counterparts, which are reviewed comprehensively in this article. Additionally, their synthesis, modelling studies, and potential applications are discussed.

1   Introduction

The discovery of carbon nanotubes (CNTs) can be considered a prominent landmark of nanomaterials and nanotechnology. In geometry, CNTs can be formed by rolling up perfect graphene sheets. Thus, ideal CNTs are composed of hexagonal rings of carbon atoms. However, non-hexagonal rings like pentagons and heptagons usually exist in actual CNTs [1]. The pentagon, with a smaller area than a hexagon, induces a positive curvature; the heptagon, with a larger area than hexagon, induces a negative curvature. The change of curvature, together with different arrangements of the pentagons and heptagons can bend and twist the CNTs into a variety of different shapes, extending CNTs into a variety of CNT-based nanostructures, including finite CNTs (such as carbon nanocaps, carbon nanotips, and carbon nanocones) [1–3], toroidal CNTs [4], kinked CNTs [5, 6], coalescent CNTs [7] and coiled CNTs [8, 9]. Compared with the straight CNTs, these CNT-based nanostructures have diverse morphologies as well as unique and distinct physical and chemical properties, so as to extend the potential applications of CNTs. In this review, we will update current progress on different dimensional nanostructures derived from CNTs, i.e., the zero-dimensional toroidal CNTs, and

---

Address correspondence to Feng Liu, fliu@eng.utah.edu; Jijun Zhao, zhaojj@dlut.edu.cn

the one-dimensional kinked and coiled CNTs.

The toroidal CNT, a kind of zero-dimensional CNT-based nanostructure, is also known as a carbon nanotorus or carbon nanoring. A carbon nanotorus can be considered as a giant all-carbon molecule and directly used as a nanoscale device. Different methods have been proposed to fabricate the toroidal CNTs, including laser-growth method [4], ultrasonic treatments [10, 11], organic reactions [12, 13], and chemical vapor deposition (CVD) [14, 15]. Theoretical studies have also been carried out to construct structural models of the toroidal CNTs. Generally, there are three kinds of toroidal CNTs: the first one consists of pure hexagonal carbon networks; the second one incorporates a certain amount of pentagons and heptagons into the hexagon carbon networks; and the third one contains only pentagons and heptagons without hexagons. Due to the circular geometry and/or presence of pentagonal and heptagonal defects, toroidal CNTs may exhibit different mechanical, electronic and magnetic properties from the straight CNTs, and hence have different potential applications.

Another kind of curved CNT-based nanostructure is the kinked CNT, which can be regarded as the joining together of different CNT pieces. The kinked CNTs are usually observed in the CNT samples made by CVD methods [16, 17]. Also, they can be obtained by directly bending the straight CNTs with an atomic force microscope (AFM) [5, 18, 19]. As for the formation mechanism of the kinked CNTs, it is believed that creation of paired pentagonal and heptagonal carbon rings is a key factor in producing this kind of nanostructure [20, 21]. Similarly, structural models of the kinked CNTs can be also built by bending the pristine CNTs or introducing pentagon–heptagon defects to form a one-dimensional kinked geometry. Generally, the pentagons and heptagons will degrade the mechanical properties of the kinked CNTs in comparison with the straight CNTs, by reducing Young's modulus (E) and intrinsic strength (τ). Moreover, the kinked CNTs will present different electronic properties from their straight CNT counterparts, because electrons can be localized at the kinked site. Most interestingly, the kinks can enhance the local chemical reactivity relative to the straight parts of nanotubes, which is potentially useful for applications in materials chemistry.

The third kind is the spiral one-dimensional carbon nanostructure, called coiled CNTs, which are also known as carbon nanocoils or carbon nanosprings. In terms of their geometry, the first two kinds of CNT-based nanostructures are planar structures, involving only bending of CNTs, but the coiled CNT can spiral in a three-dimensional space, involving twisting of CNTs in addition to bending to form a certain spiral angle resembling a spring. Due to the spring-like geometry, many studies have focused on the mechanical properties of the coiled CNTs. For fabrication of the coiled CNTs, the CVD approach showed high quality and good controllability compared with other methods [22–26]. Theoretically, various methods have been put forward to build structural models of the coiled CNTs. An important feature of the carbon nanocoil models is the periodic arrangement pentagons and heptagons in the hexagonal network. As for potential applications, because of their excellent mechanical properties, the coiled CNTs are considered as promising components in sensors, electromagnetic nanotransformers or nanoswitches, and energy storage devices.

CNTs have been well studied and many excellent reviews [27–30] and books [31–34] have covered the structures, properties and applications of CNTs. In contrast, despite of the massive amount of research devoted to CNTs with pentagons and heptagons, only a few reviews have been published on the topic of CNT-based nanostructures with incorporation of pentagons and heptagons, such as coiled CNTs [35–39]. Our motivation for writing this review is to give an overview of recent progress in this fascinating field and fill the void of different dimensional nanostructures in addition to the one-dimensional coiled CNTs, especially focusing on understanding the role of pentagons and heptagons and elaborating on their potential applications in nanodevices.

2 Zero-dimensional nanostructures: Toroidal CNTs

2.1 Fabrication and characterization

Several years after the synthesis of CNTs, toroidal CNTs were produced and characterized. Using the

laser growth method, Liu et al. pioneered the fabrication of toroidal CNTs in 1997, with typical diameters between 300 and 500 nm and widths of 5–15 nm [4]. Scanning force microscopy (SFM) and transmission electron microscopy (TEM) measurements showed that the toroidal CNTs were formed by single-walled CNT (SWNT) ropes consisting of 10 to 100 individual nanotubes. In 1999, Martel et al. reported toroidal CNTs with typical diameters of a few hundred nanometers through an ultrasound-aided acid treatment [10, 11], and Ahlskog et al. found toroidal CNTs in the CNT samples prepared by catalytically thermal decomposition of hydrocarbon gas [40]. Afterwards, other methods were also developed to fabricate toroidal CNTs, including organic reactions [12, 13] and organic-aided assembly [41], CVD methods [14, 15], and depositing hydrocarbon films in Tokamak T-10 [42]. On the other hand, different kinds of toroidal CNTs were achieved experimentally, such as incomplete

toroidal CNTs [43], Q-shaped toroidal CNTs [44], and patterning of toroidal CNTs [41, 45, 46]. In addition to the changeable shape, the tubular diameter (D_t) of a toroidal CNT is also controllable. Toroidal CNTs may be formed from single-walled [10–13, 47, 48], double-walled [49], triple-walled [50], or multi-walled CNTs [40]. Figure 1 illustrates the various kinds of toroidal CNTs reported in the literature, adapted from Ref. [39].

For experimental characterization, microscopy techniques are the main methods to reveal the structures of the toroidal CNTs, including TEM [4, 10, 11, 14, 49], AFM [12, 15, 40, 41, 43], SFM [4], and scanning electron microscopy (SEM) [11, 13, 14, 40, 45, 48, 50]. Also, some spectroscopic techniques were used to characterize the toroidal CNTs [49, 50]. For example, it was found that for straight CNT bundles, most of the diffracted intensity of the electron diffraction (ED) pattern is concentrated along the equatorial line (EL) perpendicular to the tube axis, while in the case of the
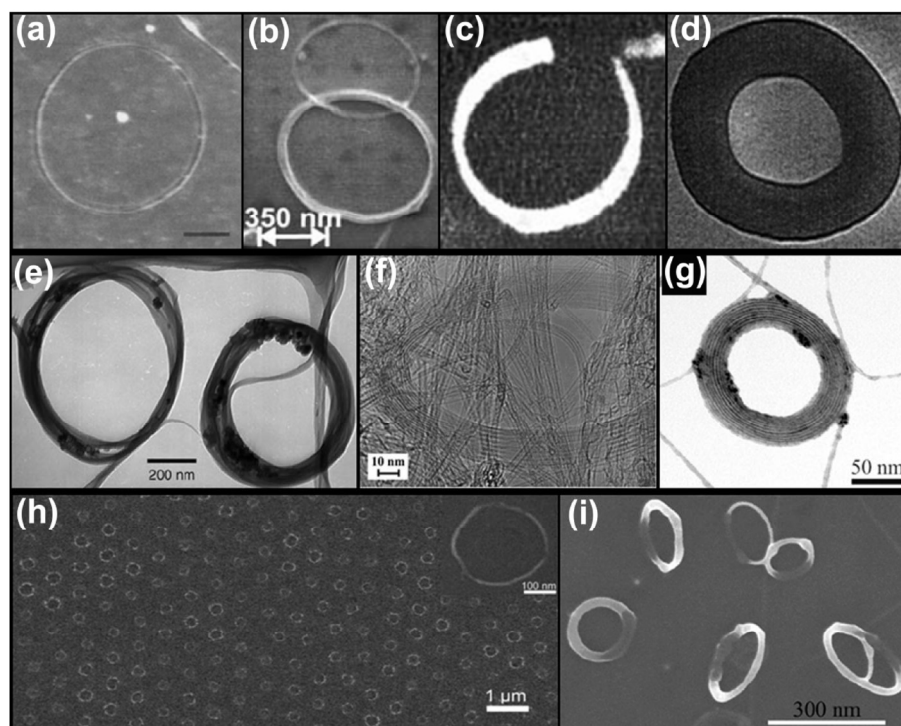

Figure 1 Experimental fabrication of various kinds of toroidal CNTs. (a) is reproduced with permission from Ref. [4]. Copyright 1997 Nature Publishing Group. (b) is reproduced with permission from Ref. [11]. Copyright 1999 American Chemical Society. (c) is reproduced with permission from Ref. [43]. Copyright 2001 Elsevier. (d) is reproduced with permission from Ref. [44]. Copyright 2004 Elsevier. (e) is reproduced with permission from Ref. [47]. Copyright 2006 Elsevier. (f) is reproduced with permission from Ref. [49]. Copyright 2003 American Chemical Society. (g) and (i) are reproduced with permission from Ref. [14]. Copyright 2006 WILEY-VCH Verlag GmbH & Co. KGaA, Weinheim. (h) is reproduced with permission from Ref. [45]. Copyright 2009 American Chemical Society.

toroidal CNTs, the ED pattern presents several lines forming rays around the (000) central beam where Bragg spots generated by the packing of the tubes inside the bundle are clearly visible [49]. Raman spectra of the toroidal CNTs showed two features: the radial breathing modes and the G tangential stretching modes [14, 45].

To understand the formation mechanism of the toroidal CNTs, Liu et al. [4] proposed a Kekuléan growth model, which was previously used to explain the formation of benzene. They suggested that during the growth process of a single CNT, it can bend around its ends in some cases. After its two ends touch together, they will align to maximize van der Waals interaction but slide over one another to release strain. Such alignment may make the touch point split again, but occasionally the closed hemi-fullerene end may stick to a catalyst particle. At a growth temperature of 1,500 K, the two ends weld together with the aid of the catalyst particle and form a seamless toroidal CNT. After that, the toroidal CNT stops growing since there is no more edge. In addition, combining the experimental measurements and a simple continuum elastic model, it was suggested that formation of the toroidal CNTs involves a balance between the tube–tube van der Waals adhesion, the strain energy resulting from the coiling-induced curvature and the strong interaction with the substrate [11, 43].

2.2 Structural models and thermodynamic stabilities

Theoretical studies of toroidal CNTs even predate their experimental fabrication. In 1992, Dunlap proposed a method to construct structural models of toroidal CNTs by connecting two SWNTs of different diameters with the inclusion of pentagons and heptagons [51]. Soon after, it was found that a C_{360} carbon nanotorus can be built from the C_{60} fullerene through introducing heptagons [52]. Based on the C_{60} fullerene, a series of toroidal CNTs with 120 to 1,920 carbon atoms can be further generated using Goldberg's prescription [53, 54]. Thereafter, numerous approaches were proposed to build the toroidal CNTs and most of them incorporate pentagons and heptagons. Generally, the approaches to construct the structural models of toroidal CNTs can be classified into six

major kinds: (1) bending a finite CNT and jointing its two ends together [55–58]; (2) connecting CNTs with different diameters by introducing pentagons and heptagons [51, 59–61]; (3) constructing from fullerenes by the Goldberg's prescription [52–54]; (4) building through the connection of one zigzag-edged chain of hexagons and another armchair-edged chain of hexagons [62]; (5) sewing the walls of a double-walled CNT at both ends [63]; and (6) constructing from pentagons and heptagons only [64]. As a consequence, there are three kinds of toroidal CNTs constructed from the above six approaches. The first one retains pure hexagonal networks, such as bending the straight CNT. The second one contains pentagons, hexagons and heptagons, for example, by introducing pentagons and heptagons into a pristine CNT. The third one has only pentagons and heptagons. In terms of radial and height dimensions, Itoh et al. classified the toroidal CNTs into five types using the parameters of the inner radius (r_i), outer radius (r_o), and height (h) [65]. Figure 2 shows these five types of toroidal CNTs, which are marked from A to E where type (A) carbon nanotorus has $r_i \approx r_o$, $h \ll r_i$, and $h \approx (r_o - r_i)$, type (B) has $r_i \sim r_o \sim h$ and $h \approx (r_o - r_i)$, type (C) has $h \ll (r_o - r_i)$, type (D) has $r_i < r_o$, $r_o \sim h$, and $h \sim (r_o - r_i)$, and type (E) has $(r_o - r_i) \ll h$.

Studying the thermodynamic stabilities of these toroidal CNT models is important to understand their existence. Several studies demonstrated that toroidal
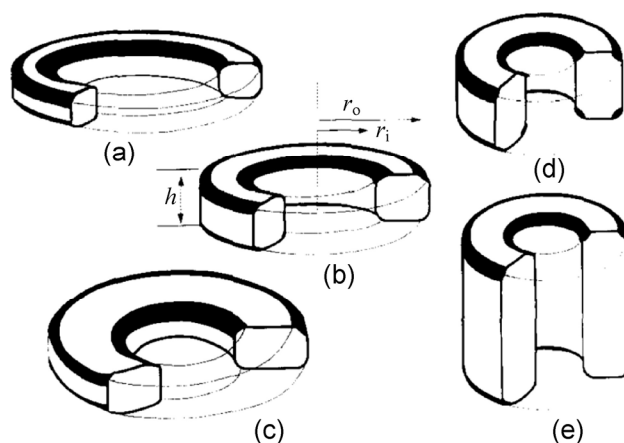
Figure 2 A schematic diagram of five types of toroidal CNTs classified by the parameters of the inner radius r_i, the outer radius r_o, and the height h. Reproduced with permission from Ref. [65]. Copyright 1995 Elsevier.

CNTs are more stable than the C_{60} fullerene by comparing their binding/cohesive energies calculated from empirical potentials [51–54]. Also, molecular dynamics (MD) simulations suggested that toroidal CNTs can survive at high temperatures up to 2,000 K [52, 58, 66, 67]. Furthermore, previous studies showed that the thermodynamic stability of a carbon nanotorus depends on its size and geometric parameters, such as total number of carbon atoms, ring diameter (D_r), tubular diameter (D_t), symmetry, curvature, and position of the pentagons and heptagons. Ihara et al. demonstrated that as the number of carbon atoms increases from 120 to 1,920, the cohesive energy of a carbon nanotorus derived from a C_{60} fullerene increases from 7.33 to 7.43 eV/atom, gradually approaching to that of graphite (7.44 eV/atom) [53]. On the other hand, the D_r and D_t can also affect the thermodynamic stability of a carbon nanotorus [68–70]. At a fixed D_t, there is a preferable D_r where the nanotorus possesses the lowest formation energy [68]. In addition, the dependence of stability on rotational symmetry was reported for the toroidal CNTs [61, 65]. Among the toroidal CNTs constructed from (5, 5), (6, 6), and (7, 7) armchair CNTs, the one with D_{6h} symmetry is energetically most favourable, as presented in Fig. 3 [61]. It was believed that [71, 72] for the toroidal CNTs with large D_r, the pure hexagonal structure is thermodynamically more stable, but for the ones with small D_r, the mixture of hexagonal networks

and pentagon-heptagon defects is favourable. Meunier et al. [72] derived an equation for determining this critical ring diameter as $D_{rc} = \pi r^2 E / (4\sigma)$, where r is the tubular radius of the initial CNT, E is the Young's modulus of the initial CNT, and σ is the surface tension of graphite perpendicular to the basal plane. For example, taking $E = 1.0$ TPa, $D_{rc} = 90$ nm can be obtained for a carbon nanotorus made of a (10, 10) nanotube with $r = 0.68$ nm. Employing MD simulations, Chang and Chou investigated both armchair and zigzag toroidal CNTs with various D_t and D_r [73]. They found that the structural stability of a perfect carbon nanotorus primarily depends on the D_t and D_r, whereas its chirality has little effect. For each D_t, there also exists a D_{rc} beyond which the perfect toroidal CNTs can form and the D_{rc} can be determined by an empirical formula:

$$D_{rc} = 0.502(2r)^2 - 3.541(2r) + 10.937 \qquad (1)$$

2.3 Mechanical properties

Chen et al. [74] investigated the mechanical properties of the zero-dimensional nanotorus, one-dimensional nanochain and two-dimensional nanomaile constructed from toroidal CNTs using MD simulations with a reactive force field. The Young's modulus E for a nanochain was found to increase monotonically with tensile strain from 19.43 GPa (strain smaller than 20%) to 121.94 GPa (strain larger than 25%) for the case of
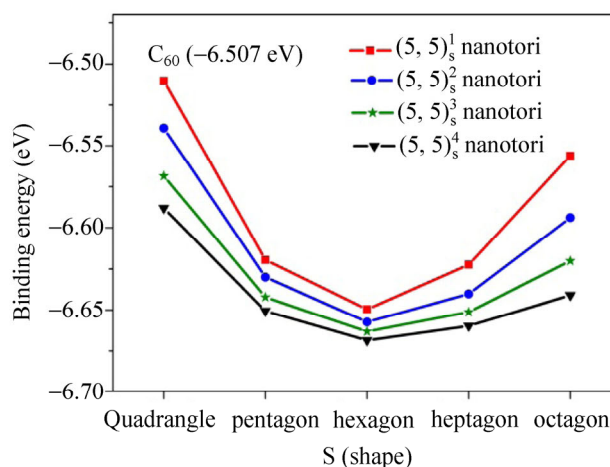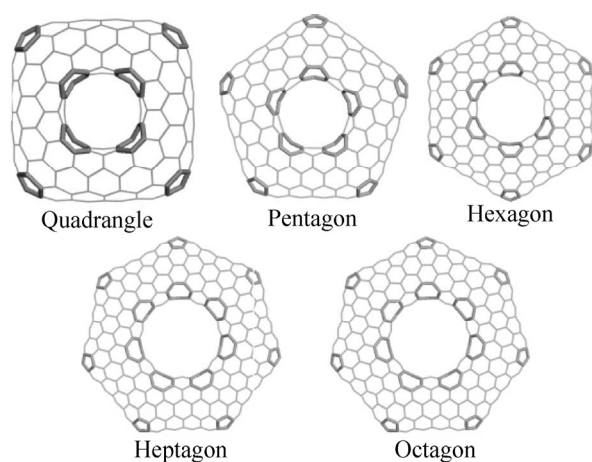

Figure 3 Different shapes of the toroidal CNTs built from (5, 5) SWNTs where each heptagon is separated by one hexagon, i.e., $(5, 5)_S^1$ (left), and the binding energies of toroidal CNTs $(5, 5)_S^n$ (right). The superscript n is the number of hexagons between two neighbouring heptagons and the subscript S is the shape of the toroidal CNT. Reproduced with permission from Ref. [61]. Copyright 2011 Elsevier.

without any side constraints. However, if there are side constraints, the E becomes much larger, increasing from 124.98 GPa to 1,559.9 GPa with tensile strain. Here the side constraint means fixing the position of small regions of carbon atoms on left and right sides. The tensile strength of the unconstrained and constrained nanotorus was estimated to be 5.72 GPa and 8.52 GPa, respectively. The maximum elastic strain (ε_c) is approximate 39% for the nanochain and 25.2% for the nanomaile. For a nanotorus obtained from bending a (10, 10) CNT, its E along the tube axis was 913 GPa by taking r_o = 16.7 Å [75]. Also, using molecular mechanics (MM) computations, the buckling behavior of toroidal CNTs under tension was investigated, including the toroidal CNTs formed from (5, 5), (8, 8) and (9, 0) CNTs [76, 77]. It was found that the buckling shapes of the toroidal CNTs constructed from both armchair and zigzag CNTs with an odd number of units are unsymmetrical, whereas those with an even number of units are symmetrical. Recently, geometric reversibility of the toroidal CNTs under strain has been predicted theoretically by employing a nonlinear continuum elastic model [78, 79]. Most interestingly, the reversible elastic transformation between the circular and compressed toroidal CNTs in a colloid was observed by Chen et al. using TEM [46], suggesting the potential applications of toroidal CNTs as ultrasensitive force sensors and flexible and stretchable nanodevices.

2.4 Electronic properties

It is well-known that the geometry of a CNT can be described by a chiral vector $C_h(n, m)$ and a translation vector $T(p, q)$. Depending on the chirality, it is either metallic or semiconducting [33]. Since the toroidal CNT can be built from a straight CNT through bending or introducing pentagons and heptagons, it would be interesting to explore how the electronic properties of toroidal CNTs are varied by the bending and the inclusion of pentagons and heptagons.

For a carbon nanotorus built from bending a (*n*, *m*) CNT, similar to the CNTs, its electronic structure can be determined according to the C_h (n, m) and T (*p*, *q*) vectors. If $m - n = 3i$ and $p - q = 3i$ (*i* is an integer), the carbon nanotorus is metallic; if $m - n = 3i$ and $p - q \neq 3i$, and $m - n \neq 3i$ and $p - q = 3i$, there is a band gap; and for the case of $m - n \neq 3i$ and $p - q \neq 3i$, no carbon

nanotorus exists [80]. This classification was shown by Ceulemans et al. [81] using tight-binding (TB) calculations. They found that a metallic carbon nanotorus can be constructed by bending a metallic CNT and also follows the rule of divisibility by three on the indices of chiral and translation vectors. Moreover, delocalized and localized deformations play different roles on the electronic properties of a carbon nanotorus built from bending a CNT [56]. The delocalized deformations only slightly reduce the electrical conductance, while the localized deformations will dramatically lower the conductance even at relatively small bending angles. Here the delocalized deformation means the deformation induced by the mechanical bending of the CNT, which is usually reversible; the localized deformation indicates the deformation induced by the pushing action of an AFM tip that is irreversible and makes electrons be localized at the deformed region. In addition, Liu and Ding reported the electronic properties of the toroidal CNTs built from both armchair and zigzag CNTs [82]. They found that as the number of carbon atoms of a toroidal CNT increases, there is an oscillation in the energy gap. When the number of carbon atoms becomes sufficiently large, the gap will eventually converge to that of the infinite CNT.

On the other hand, for toroidal CNTs with pentagons and heptagons, an energy gap between the highest occupied molecular orbital (HOMO) and lowest unoccupied molecular orbital (LUMO) can be expected, because of charge localization at the pentagonal and heptagonal defect sites. For a carbon nanotorus C_{1960} constructed by connecting (6, 6) and (10, 0) CNTs, a HOMO–LUMO gap of 0.05 eV was predicted by a TB approach [72]. Employing the TB and semiempirical quantum chemical approaches, a series of toroidal CNTs with total number of atoms ranging from 120 to 768 were investigated and most of them have a HOMO–LUMO gap around 0.30 eV [83]. For the toroidal CNTs of C_{170}, C_{250}, C_{360}, C_{520}, and C_{750}, a varying HOMO–LUMO gap from 0.04 to 0.32 eV was predicted by Yazgan et al. using the extended-Hückel method [84]. More accurate density functional theory (DFT) calculations showed that the carbon nanotorus C_{444} has a gap of 0.079 eV and the nanotorus C_{672} has a gap of 0.063 eV, respectively [85].

2.5 Magnetic properties

Due to the unique circular geometry of toroidal CNTs, it is interesting to explore their magnetic properties and the magnetic response when a ring current flows in a carbon nanotorus. Early in 1997, Haddon predicted that the nanotorus C_{576} has an extremely large and anisotropic ring-current diamagnetic susceptibility, which is 130 times larger than that of the benzene molecule [86]. Later, Liu et al. [57] predicted the colossal paramagnetic moments in the metallic toroidal CNTs, which were generated by the interplay between the toroidal geometry and the ballistic motion of the π-electrons, as plotted in Fig. 4. For example, the nanotorus C_{5100} built from a (5, 5) CNT possesses a large paramagnetic moment of 296.8 μ_B at 0 K. Similarly, the nanotorus C_{5580} built from a (7, 4) CNT has a giant zero-temperature magnetic moment of 304.3 μ_B. In addition to the paramagnetic moments, existence of ferromagnetic moments at low temperatures in the toroidal CNTs without heteroatoms was also predicted by using a π-orbital nearest-neighbour TB Hamiltonian with the London approximation, which is attributed to the presence of pentagons and heptagons [87]. Another important phenomenon, the Aharonov–Bohm (AB) effect was predicted from a theoretical point of view to be observable in the toroidal CNTs [88–92]. It was shown that a persistent current can be created by the magnetic flux (φ) through the toroidal CNTs [88]. The persistent current is a linear periodic function of φ, with a period of φ_0 (hc/e). Such an oscillation is the manifestation of the AB effect. Generally, the magnetic properties of the toroidal CNTs are affected by many factors. Liu et al. pointed out that the paramagnetic moments of the toroidal CNTs decrease dramatically as temperature increases [57]. Meanwhile, for toroidal CNTs with diamagnetic moments, the magnitude of moment also decreases with the increasing temperature [57]. Such temperature dependence was also shown later by several other theoretical studies [93–95]. The magnetic properties of the toroidal CNTs depend generally on the geometric parameters, such as D_r, curvature, chirality, and the arrangement of pentagons and heptagons [93–95].

2.6 Chemical modifications and applications

To improve or tailor the properties of materials for applications, chemical modification such as doping and functionalization is an effective approach. Usually, doping is an important method of chemical modification. It was found that existence of pentagons and heptagons in the toroidal CNTs is helpful for impurity doping. Liu et al. [61] demonstrated that compared with the hexagonal rings, the pentagonal sites are favoured for nitrogen doping and the heptagonal
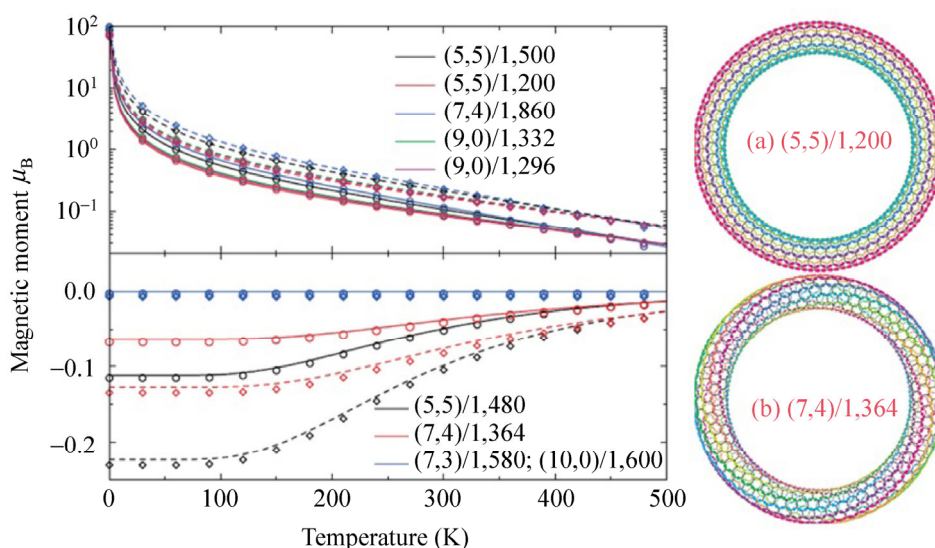

Figure 4 Induced magnetic moment as a function of temperature for various toroidal CNTs in a perpendicular magnetic field of 0.1 T (solid line) and 0.2 T (dashed line), respectively. Reproduced with permission from Ref. [57]. Copyright 2002 American Physical Society.

sites for boron doping. The substitutional doping of boron or nitrogen atoms will modify the electronic properties of the toroidal CNTs due to the change of localized charges at the defect sites. Moreover, Rodríguez-Manzo et al. found that doping electrons or holes into a carbon nanotorus could vary its magnetic properties via altering the band-filling configuration [96]. In addition to the charge and substitutional doping, atoms or molecules can be also encapsulated into the toroidal CNTs since they have the hollow tubular structures similar to the CNTs. In 2007, Hilder et al. examined the motion of a single offset atom and a C_{60} fullerene inside a carbon nanotorus to explore its application as high frequency nanoscale oscillator [97]. They demonstrated that the C_{60} fullerene encapsulated carbon nanotorus can create a high frequency up to 150 GHz, which may be controlled by changing the orbiting position. By inserting the chains of Fe, Au, and Cu atoms into a carbon nanotorus, Lusk et al. investigated the geometry, stability, and electronic and magnetic properties of this nanocomposite structure [98]. A reduced HOMO–LUMO gap and ferromagnetism of the nanotorus by encapsulating chains of metal atoms were predicted. Using the continuum approximation together with the Lennard-Jones potential, Chan et al. [99] studied the trapping effects of toroidal CNTs both on the atoms and ions, which depend on their geometric factors. Additionally, the diffusion behaviour of water molecules inside a carbon nanotorus was studied by MD simulations [100]. Intuitively, water molecules moving inside a carbon nanotorus seem to be a very appropriate system to observe single-file diffusion, where the water molecules are unable to cross each other. However, it was demonstrated that a single chain of water molecules presented normal diffusion behavior, i.e., Fickian diffusion. When water molecules form two or more polarized chains, single-file diffusion was observed [100]. On the other hand, the toroidal CNTs can be used for hydrogen storage. For the toroidal CNTs coated with beryllium, each beryllium atom can adsorb three H_2 molecules with a moderate adsorption energy of 0.2–0.3 eV/H_2 [101].

Due to their circular geometries and unique properties, the toroidal CNTs have been proposed to have applications in many fields. For example, the reversible elastic properties of the toroidal CNTs make them good candidates for ultrasensitive force sensors, and flexible and stretchable nanodevices. The toroidal CNTs are also promising candidates for electromagnetic oscillators due to their excellent magnetic properties. Moreover, the toroidal CNTs with tunable electronic properties can directly serve as nanoscale devices in integrated circuit. In particular, the tubular structure of the nanotorus is useful for trapping atoms, ions and molecules and storing hydrogen.

3 One-dimensional nanostructures: Kinked CNTs

3.1 Fabrication and formation mechanism

Kinked CNTs are made or observed in experiments. Simply, kinked CNTs can be directly bent from straight CNTs by manipulation with an AFM [5, 18, 19]. Among different kinds of kinked CNTs, the one with zigzag-shaped morphology has attracted much attention. Using a scanning probe microscopy (SPM) probe, freestanding nanotubes can be bent to the kinked CNTs with zigzag-like shapes (abbreviated as Z-CNTs hereafter), and this kinked morphology can be fixed by electron-beam-induced deposition (inside a TEM) of amorphous carbon on the bent area [102]. Also, Gao et al. synthesized the Z-CNTs using the approach of catalytic decomposition of ethylene, where the detailed morphology depends on the arrangement of pentagon–heptagon carbon rings [20]. They pointed out that if there is no twist in the pentagon–heptagon orientation along the body of carbon nanotube, a Z-CNT with a planar–spiral structure would be formed; otherwise, the helical structure would be obtained if there is a twist. By changing the direction of an applied electric field during dc plasma enhanced CVD, AuBuchon et al. obtained Z-CNTs with a bending angle of ~90° while keeping the same diameter before and after bending [16, 17]. Moreover, through catalytically producing CNTs on miscut C-plane sapphire wafers, i.e., $-Al_2O_3$ (0001) surfaces, the Z-CNTs can grow naturally due to the preferred CNT growth along the faceted atomic steps which are zigzag-shaped [21]. It was found that the atomic-scale surface features can direct the orientation and conformation,

and possibly also the structure of SWNTs. Similarly, the Z-CNTs can also be produced on quartz substrates by crinkling ultralong CNTs via controlling the landing process, where the detailed shape is determined by the lattice-alignment force and the shear friction force [103, 104]. In addition, when the CNTs are aligned into CNT arrays through substrate and feed gas, the one with the zigzag-shaped morphology can be produced by exploiting the effects of CNT–lattice interaction and gas flow orientation [105]. The unique zigzag-shaped morphology of Z-CNT may be useful for a variety of applications, including AFM tips, mechanical nano-springs and nanocircuit interconnections [16, 17, 102, 105]. Figure 5 illustrates the kinked CNTs fabricated in experiments.

Various microscopy techniques, such as AFM [5, 18, 19, 21, 103], TEM [17, 20, 102], and SEM [16, 17, 103–105], were employed to reveal the structures of the Z-CNTs. In addition, Raman spectroscopy [106, 107] showed that for the kinked CNTs, torsional strain strongly affects the Raman spectra, inducing a large downshift of the E_2 mode in the G^+ band, but a slight upshift for the rest of the modes and also an upshift in the radial breathing mode. Under the torsional strain, resonant Raman spectral mapping along a SWNT detected an

M-shaped frequency and W-shaped intensity variation of the radial-breathing-mode spectra, which were induced by elastic retraction of the nanotubes in combination with the friction after the tip has been removed [107]. Furthermore, using polarized resonant Raman spectroscopy, G-band modes with different symmetries were found to respond quite differently to torsional strain. Generally, the variation of the G-band is sensitive to the tube diameter and chirality. Also the quasiacoustic plasmon mode has a significant effect on the torsional strain-induced variation of G-band [108].

As for the mechanism of forming the Z-CNTs, Gao et al. [20] suggested that the creation of the paired pentagonal and heptagonal carbon rings is a key factor in producing various shapes of graphitic layers. The SWNT is believed to be grown from a carbon cluster (or node) that is nucleated from a pentagon carbon ring followed by a spiral shell growth. The geometrical shape of the tube is determined by the fraction and growth rate of pentagonal, hexagonal, and heptagonal carbon rings, which can be kinetically controlled. If there is no twist on the pentagon-heptagon orientation along the body of the carbon nanotube, a planar–spiral structure, i.e., Z-CNT, would
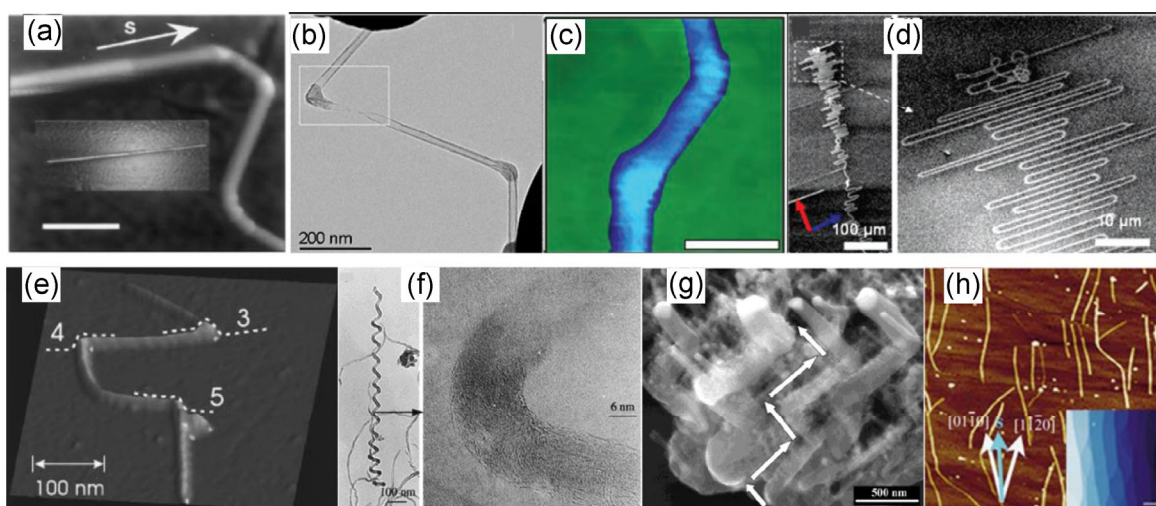

Figure 5 Various kinds of kinked CNTs fabricated in experiments. (a) is reproduced with permission from Ref. [5]. Copyright 1997 Nature Publishing Group. (b) is reproduced with permission from Ref. [102]. Copyright 2006 WILEY-VCH Verlag GmbH & Co. KGaA, Weinheim. (c) is reproduced with permission from Ref. [19]. Copyright 2001 American Association for the Advancement of Science. (d) is reproduced with permission from Ref. [105]. Copyright 2007 American Chemical Society. (e) is reproduced with permission from Ref. [18]. Copyright 1998 American Chemical Society. (f) is reproduced with permission from Ref. [20]. Copyright 2000 American Chemical Society. (g) is reproduced with permission from Ref. [16]. Copyright 2004 American Chemical Society. (h) is reproduced with permission from Ref. [21]. Copyright 2004 WILEY-VCH Verlag GmbH & Co. KGaA, Weinheim.

be formed. A straight tube would be grown if the pentagon and heptagon carbon rings are absent. Ismach et al. also suggested that pentagon–heptagon pairs contribute to the Z-CNTs [21]. They pointed out that for a Z-CNT with a bending angle of 30°, involving pentagon–heptagon defects is an energetically favoured process over bending or buckling. The energy associated with pentagon–heptagon defects was calculated to be about 7 eV, whereas the minimum strain energy required to produce a 30° buckle in a 1-nm-dimater SWNT was estimated to be about 13 eV. For the Z-CNTs formed on quartz or sapphire substrate, a "falling spaghetti" mechanism was proposed [103]. According to this mechanism, the CNTs are first catalytically synthesized while floating above the substrate and then absorbed onto the surface in a zigzag pattern from base to tip. The lattice-alignment force and the shear friction force compete to determine the geometry of the Z-CNTs. When the CNT lands, due to different absorption energy, the anisotropic quartz/sapphire surface will preferentially adsorb the CNT along its lattice direction, which results in a lattice-alignment force. On the other hand, the shear friction force between the flowing gas and the floating portion of the CNT tends to drag it straight forward. The fluctuation of the relative strength of these two forces causes the serpentine geometry of the CNTs [104].

3.2 Theoretical modelling and energy stabilities

Compared with the abundant studies of experimental synthesis, only very limited theoretical effort has been devoted to understanding the atomic structures and physical properties of Z-CNTs. To make the Z-CNTs, one way is to directly bend a SWNT into the zigzag-like morphology, as introduced by Xu and Buehler [109]. Alternatively, through connecting CNT pieces of different chiralities via pentagons and heptagons to form the kinks, Lu also constructed kinked CNTs with zigzag-like morphologies [110]. Similarly, by periodically introducing pentagons and heptagons into perfect (5, 0) and (6, 0) SWNT, Wu et al. [85] constructed step-kinked CNTs. Another approach to build the Z-CNTs is to introduce two pairs of pentagon–heptagon defects at the kinks [111], which results into Z-CNTs with different values of D_t.

Generally, introducing pentagons and heptagons into the pristine CNTs can induce curvature and lead to the zigzag-shaped morphology. Figure 6 shows the structural models of the kinked CNTs proposed by different groups.

Employing DFT calculations with the Vienna ab initio simulation package, the Z-CNTs built from pristine SWNTs are found to have comparable thermodynamic stability with the SWNTs, just about 0.05 eV/atom higher in binding/formation energies, and much more stable than the C_{60} fullerene [111].

3.3 Mechanical properties

It is known that pristine CNTs have excellent mechanical properties with an average E of ~1.0 TPa [112], a theoretical τ of ~100 GPa ± 30 GPa and a fracture strain ε_c of ~15% ± 5% [113, 114]. Recent work [111] has indicated that the existence of pentagons and heptagons in the Z-CNTs will reduce the E to several hundreds of GPa, and the τ and ε_c of the Z-CNTs are also lower than those of the pristine CNTs. Table 1 compares several mechanical parameters of the Z-CNTs and the pristine SWNTs. If we take the E and τ of graphene sheet (corresponding to a CNT of infinite radius r) as the upper limit of the (n, n) Z-CNTs, which are 1,037 and 111.8 GPa separately, the dependence of E and τ on r for the Z-CNTs was shown to follow the empirical formulae [111]:

$$E = 470 + 567 \times e^{(-6.4/r)} \tag{2}$$

Table 1 Comparison of Young's modulus E, intrinsic strength τ and fracture strain ε_c between Z-CNTs and the pristine single-walled CNTs. Reproduced with permission from Ref. [111]. Copyright 2013 Royal Society of Chemistry.

Chiral index	Z-CNTs			SWNTs		
	E (GPa)	τ (GPa)	ε_c (%)	E (GPa)	τ (GPa)	ε_c (%)
(5, 5)	561	68.7	14	908	96.0	17
(6, 6)	580	72.4	14	922	98.4	21
(7, 7)	613	76.6	14	935	103.6	20
(8, 8)	651	81.4	15	957	105.2	20

and

$$\tau = 34.7 + 77.1 \times e^{(-2.8/r)}, \tag{3}$$

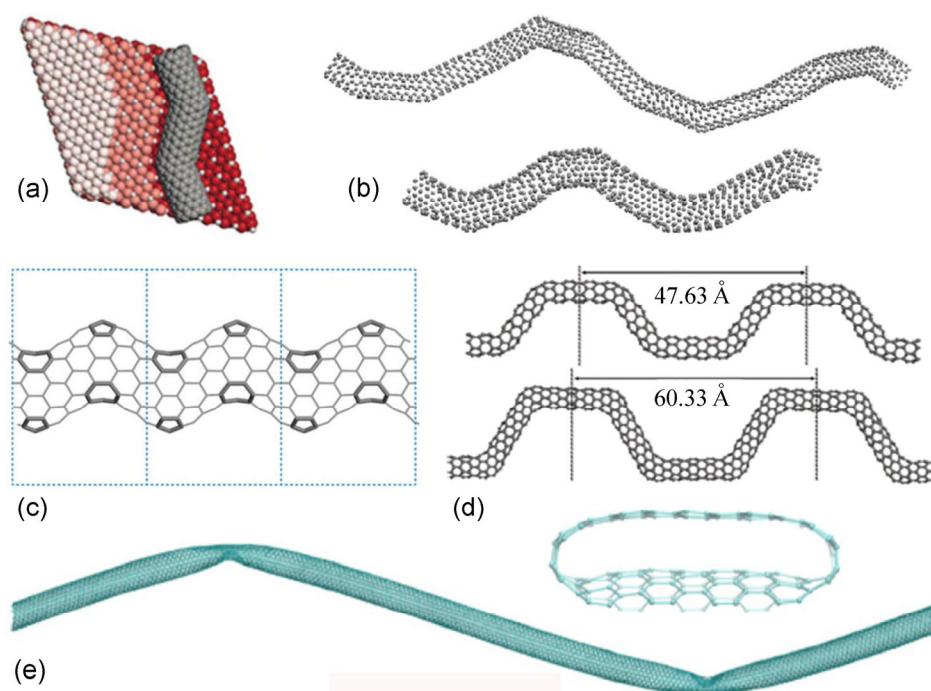where E and τ are in the unit of GPa, and r is in the

Figure 6   Several kinds of structural models proposed for kinked CNTs. (a) is reproduced with permission from Ref. [21]. Copyright 2004 WILEY-VCH Verlag GmbH & Co. KGaA, Weinheim. (b) is reproduced with permission from Ref. [110]. Copyright 2005 Elsevier. (c) is reproduced with permission from Ref. [111]. Copyright 2013 Royal Society of Chemistry. (d) is reproduced with permission from Ref. [85]. Copyright 2011 American Chemical Society. (e) is reproduced with permission from Ref. [109]. Copyright 2009 IOP Publishing Ltd.

unit of Å. In addition, when the Z-CNTs were stretched to the maximum strain, the first fractured bond is a distorted sp^2 C–C bond shared by a hexagon and another heptagon (namely, the 6–7 bond).

3.4   Electronic properties

Due to their kinked structure, the Z-CNTs exhibit different electronic properties from those of the pristine CNTs. Using scanning tunneling microscopy (STM) and scanning tunneling spectroscopy (STS), Tekleab et al. [115] measured the local density of states (LDOS) of kinked multi-walled CNTs and found that the LDOS is asymmetric about the Fermi level, while the spectra from regions away from the kink exhibit the usual symmetric LDOS as in perfect tubes. In the kinked region, the distribution of the unoccupied states is suppressed and the intertube wall slippage due to deformation opens a pseudogap. In particular, the zigzag-shaped kinks can make CNTs as single-electron transistors [19]. On the other hand, using a

π-orbital tight-binding model and the Green's function approach, Lu investigated the transport properties of kinked CNTs and found that incorporation of pentagons and heptagons can make the conductance of kinked CNTs quantized due to electron scattering [110]. Employing DFT calculations, Wu et al. investigated the electronic properties of step-kinked CNTs and predicted that pentagons and heptagons may either keep the metallicity of the pristine CNTs or transform the metallic CNTs into semiconductors [85]. In agreement with Wu et al.'s results, Liu et al. [111] found introducing pentagons and heptagons in the (5, 5), (7, 7), and (8, 8) Z-CNTs will make them semiconducting; but the (6, 6) Z-CNTs with pentagons/heptagons remain metallic like the (6, 6) SWNT. Under uniaxial tensile strain, all these Z-CNTs exhibit significant electromechanical coupling effect with a semiconductor–metal or metal–semiconductor transition. This electromechanical coupling effect is somewhat different from those in pristine CNTs [116–119], which can be explained by the change of

partial charge density near Fermi energy. Taking the (5, 5) Z-CNT as an example, charges distributions on the valence band maximum (VBM) and conduction band minimum (CBM) of the (5, 5) Z-CNT at the equilibrium state are mainly localized at the pentagonal and heptagonal sites, where large curvature introduces distorted sp^2 hybridization. As the (5, 5) Z-CNT is elongated, the localized charges at the heptagonal sites are gradually delocalized, leading to shrinkage of band gap and eventually a semiconductor–metal transition at a tensile strain of 14%, as shown in Fig. 7 [111].

3.5   Chemical and other properties

As mentioned above, the kinked part can trap electrons and thus induce some new properties different from that of the straight CNTs [115]. By investigating the chemisorption of hydrogen atoms, it was found that kinks and other nonlinear/irreversible distortions may act as sites of enhanced chemical reactivity, as evidenced by the energy of a hydrogen atom chemisorbed to those sites near the regions of local nonlinear distortions which was predicted to be enhanced by as much as 1.6 eV relative to unstrained nanotubes [120]. Recently, Liu et al. [111] demonstrated the localized charges at pentagonal and heptagonal sites. The localized charges at the pentagons and heptagons can

make the Z-CNTs useful for chemisorption of atoms, molecules and clusters. Moreover, the tensile strain can change the localized charges at defective sites, which may further affect the chemisorption and even lead to a tunable chemisorption/chemidesorption property.

In addition, the kinked structure can lower the thermal conductivity of the CNT due to the increased scattering by shortening of the phonon mean free path and interface resistance, which arises from the localized buckling [109]. When torsional strain is applied, the thermal conductivity drops as well, with significant reductions once the carbon nanotube begins to buckle, i.e. forming kinked structure, as predicted by Xu and Buehler [109].

3.6   Applications

The unique Z-CNTs with zigzag-shaped morphology can be useful for a variety of applications. As reported by Postma et al. [19], by bending a metallic CNT into the zigzag shape with two kinks, the conductance at the kinks will be suppressed and differ from the unstained nanotubes. This makes the kinked CNTs as single-electron transistors. The kinked CNTs may also be good candidates for bent mass-transport channels. When liquid passes through the bent region, the gradually bent channel may cushion the momentum transfer of the passing liquid. In addition, the kinked
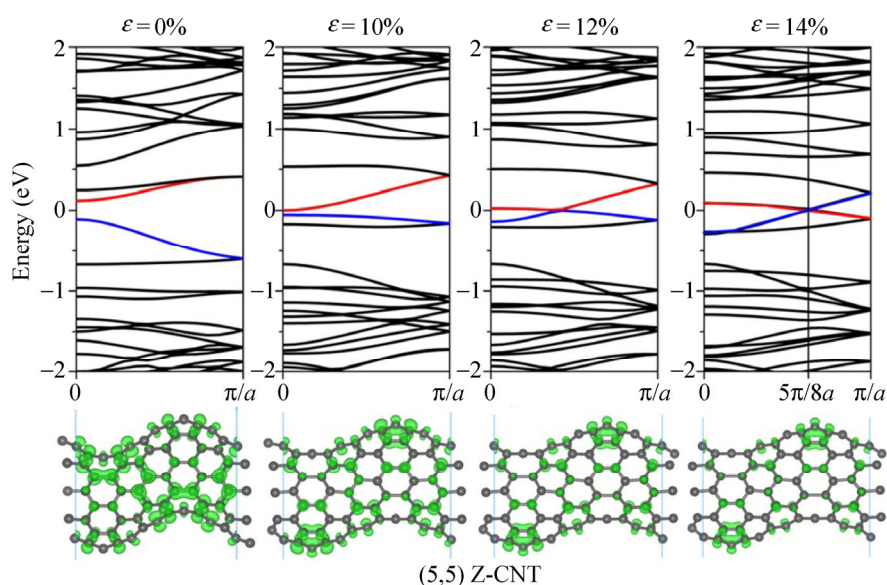

Figure 7   Change of band structures under a uniaxial tensile strain and the corresponding variation of partial charge density at the VBM and CBM for the (5, 5) Z-CNT. Reproduced with permission from Ref. [111]. Copyright 2013 Royal Society of Chemistry.

CNTs can be used as mechanical nanosprings and AFM tips to detect some complicated topographies that are inaccessible to straight CNTs [102]. Since the kinked CNTs can keep the metallic character of pristine CNTs [85, 102, 111], they are also potentially useful for complicated circuit nanointerconnections. Especially, the strain-induced sensitive change of electronic properties from semiconductor to metal or metal to semiconductor enables the kinked CNTs as promising electromechanical sensors or switches in nanoelectromechanical systems (NEMS) [111].

3.7 Zigzag-shaped graphene nanoribbons

Similar to the Z-CNTs, graphene nanoribbons (GNRs) can also form the zigzag-shaped structures, as shown in Fig. 8. In 2008, Li et al. developed a chemical route to produce GNRs with width below 10 nm and obtained the zigzag-shaped graphene junctions [121]. In addition, through Joule heating and electron beam irradiation, Jia et al. demonstrated that zigzag-shaped graphene junctions can be formed by edge-reconstruction process [122]. Later, using TEM to examine the edges of multi-layer graphene sheets, Warner et al. also identified the zigzag-shaped graphene edges with sawtooth oscillations in the atomic structure with zigzag edge terminations along the general armchair direction [123]. In 2010, Cai et al. [124] were able to produce zigzag-shaped GNRs (Z-GNRs)

through a bottom-up fabrication process. By tuning the functionality pattern of the precursor monomers, they fabricated GNRs with complex shapes.

Compared with the straight GNRs, the Z-GNRs or sawtooth GNRs present some different properties. Employing DFT calculations, it was found that the unique edge structures of the Z-GNRs induce richer band-gap features than the straight GNR counterparts with either armchair or zigzag edges [125]. The Z-GNRs with only zigzag edges are generally semiconducting with direct band gaps, which depend on both the nanoribbon's width and the period. Different from straight GNRs, for Z-GNRs with only zigzag edges, an external electric field can only affect the band structure and the position of the Fermi level, but cannot lead to half metallicity. However, things are little different for the Z-GNRs comprising hybrid GNR segments with alternating armchair and zigzag edges [126]. For the hybrid Z-GNRs consisting of both armchair and zigzag GNRs, the combined electronic band structures lead to a band gap which is insensitive to system size and only increases slightly when the ribbon width initially increases [126]. However, under an external electric field, band structures of the Z-GNRs will be changed, and with increasing field strength, the spin-up gap gradually increases while the spin-down gap reduces quickly and eventually leads to the half-metallicity. Calculations of transport
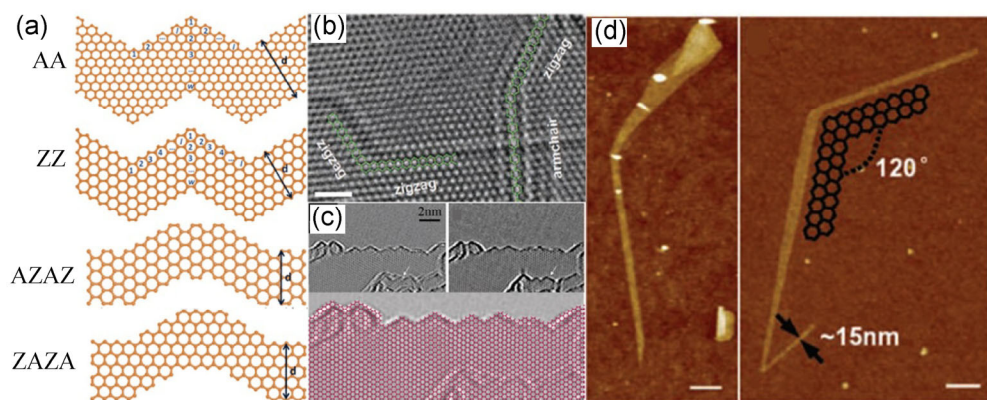

Figure 8 Various structures of the Z-GNRs. (a) Four kinds of Z-GNRs with different edges, including armchair–armchair edges (AA), zigzag–zigzag edges (ZZ), armchair–zigzag edges (AZAZ) and zigzag–armchair edges (ZAZA). Reproduced with permission from Ref. [133]. Copyright 2011 American Physical Society; and (b), (c) and (d) show experimental fabrication of the Z-GNRs. (b) is reproduced with permission from Ref. [122]. Copyright 2009 American Association for the Advancement of Science. (c) is reproduced with permission from Ref. [123]. Copyright 2009 American Chemical Society. (d) is reproduced with permission from Ref. [121]. Copyright 2008 American Association for the Advancement of Science.

properties show that the unique band structure of the Z-GNRs produces asymmetric spin-transmission coefficients which cause unequal currents in different spin channels [126]. Also, a zigzag–armchair–zigzag Z-GNR can form a nanoscale field effect transistor consisting of a metal–semiconductor–metal junction [127]. In addition, the zero-dimensional Z-GNR junctions can serve as quantum dots, which can completely confine electronic states induced by the topological structure of the junction [128], and be used as building blocks to construct quantum cellular automata for computing [129]. One the other hand, the Z-GNRs also possess different magnetic properties from their straight GNR counterparts. Yu et al. introduced a unified geometric rule for designing magnetic GNR by changing the relative orientations of the two edges [130]. It was shown that any two zigzag edges will be ferromagnetically coupled if they are at an angle of 0° or 120° and antiferromagnetically coupled at an angle of 60° or 180°. Furthermore, when the Z-GNRs are under a transverse electrical field, they become a spin semiconductor where charge carriers are not only spin polarized in energy space but also spatially separated at different edges [131]. The spatially separated spin carriers at different edges, which also show a high degree of tunability by electric field and robustness against edge disorder, are very useful for potential spintronics applications. For the Z-GNRs with hybrid zigzag–armchair edges, with the increasing length of the zigzag segments, the nonmagnetic semiconducting Z-GNRs can be converted to spin-polarized semiconductors with a antiferromagnetic ground state [132]. In addition to the electronic and magnetic properties, the Z-GNRs also have enhanced thermoelectric properties compared with the straight GNRs. It was found that for Z-GNRs with armchair edges, the first peak of the figure of merit (ZT_{max}) is almost twice than that of straight GNRs with armchair edges, while for Z-GNRs with zigzag edges, ZT_{max} is greatly improved from that of straight GNRs with zigzag edges, which is around zero [133]. The higher figure of merit of the Z-GNRs is partly due to their smaller thermal conductivity than that of straight armchair-GNRs, as the rougher edges increase lattice scattering of phonons [134]. Moreover, the thermal conductivity of Z-GNRs is found to be nearly independent on the length, but sensitive to the width.

4   One-dimensional nanostructures: Coiled CNTs

4.1   Fabrication and formation mechanism

As early as 1994, the coiled CNTs were experimentally produced by catalytic decomposition of acetylene over silica-supported Co catalyst at 700 °C [8, 9]. The unique spiral structure attracted much attention and numerous methods have followed to synthesize the coiled CNTs, including laser evaporation of a fullerene/Ni particle mixture in vacuum [135], opposed flow flame combustion of fuel and the oxidizer streams [136], electrolysis of graphite in fused NaCl at 810 °C [137], self-assembly from π-conjugated building blocks [138, 139], and CVD methods [22–26]. Among them, the CVD approach is predominant due to its high quality products, and has been previously reviewed [35, 38, 140]. To fabricate the coiled CNTs, the CVD process involves the pyrolysis of a hydrocarbon (e.g., methane, acetylene, benzene, propane) over transition metal catalysts (e.g., Fe, Co, Ni) at high temperatures. Compared to the high growth temperature (>2,000 °C) of CNTs in arc discharge and laser evaporation processes, the relatively low growth temperature of the CVD method (500–1,000 °C) allows carbon atoms move slowly and form non-hexagonal carbon rings [35]. As summarized by Lau et al., there are three major CVD-based methods to fabricate coiled CNTs, including catalyst-supported CVD growth, on-substrate CVD growth and template-based CVD growth [35]. During the CVD process, several synthetic parameters play important roles in growth of the coiled CNTs, such as catalyst, gas atmosphere and temperature, and these have been discussed by Fejes et al. [140] and Shaikjee et al. [38]. By adjusting the concentration of carboxylic acid metal salts in the solution, the sizes of the catalyst particles can be tailored to afford controllable coiled CNTs. It was found that the inner coil diameter (D_i) of the nanocoils is proportional to the radius of the catalyst particles (r_p), which can be expressed by $D_i = 2r_p / (v_o / v_i - 1)$ where v_o and v_i are the velocities of the carbon extrusion from the outer

and inner sides of the catalyst particle ($v_o > v_i$) [141]. Particularly, the coiled CNTs with good helical structures can grow on a catalytic particle with the diameter <150 nm, whereas a carbon nanocoil with a straight segment extruded at the end of growth can grow on a catalytic particle with the diameter ranging from 150 to 200 nm. For catalytic particles with a diameter larger than 250 nm, a CNT bundle can be obtained [26]. In addition, at low temperature (700–770 °C), one-dimensional coiled CNTs are produced, while a higher temperature (810 °C) leads to the growth of straight carbon nanofibers [142]. Moreover, change of gas atmosphere, such as the pulse and flow rate, is effective in controlling the structure of coiled CNTs. It was found that higher flow rates of acetylene result in smaller coil pitch (λ) and diameter of the carbon nanocoils [142]. Figure 9 presents different types of the coiled CNTs with non-linear morphology, as reported by Shaikjee et al. [38]. Among various characterization techniques, microscopy techniques, such as TEM [9, 20, 26, 143, 144] and SEM [145], are the main approaches to reveal the structures of coiled CNTs. Furthermore, other techniques, including ED [146, 147], Raman spectra [24, 26, 137, 148, 149], and X-ray diffraction (XRD) [24, 150–152], have also been
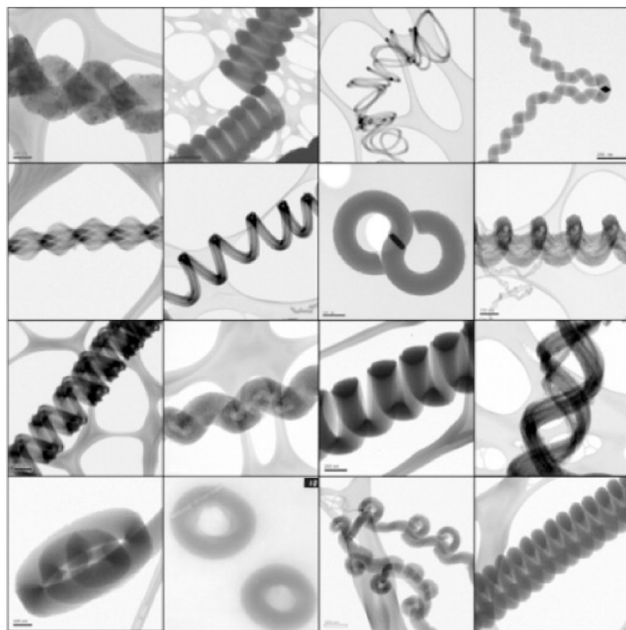
used to get further insight into the structures of coiled CNTs.

To understand formation of the coiled CNTs, several mechanisms have been proposed. Generally, formation of the coiled CNTs is closely related to the catalyst. Amelinckx et al. proposed a growth mechanism for the carbon nanocoils based on the mismatch between the extrusion velocities of carbon from the catalyst grain [8]. Kuzuya et al. suggested that growth of the carbon microcoils is based on the anisotropic deposition rate between the catalyst crystal faces [153]. Fonseca et al. presented formation of (chiral and achiral) knees on a catalyst particle to further form toroidal and coiled CNTs, which can be described by a simple formalism using the heptagon–pentagon construction [154]. Pan et al. suggested that the catalyst grain is crucial to the geometry of a carbon nanocoil, and the nonuniformity of carbon extrusion speed in the different parts of the catalyst grain leads to the helical growth of the coiled CNTs [145]. Chen et al. pointed out that the driving force of coiling straight CNTs was the strong catalytic anisotropy of carbon deposition between different crystal faces [155]. For growth of carbon microcoils, the catalyst grain rotates around the coil axis which is on the symmetric face of the deposition faces, while for the twisted carbon nanocoils, the catalyst grain rotates around the axis which is perpendicular to the symmetric face of the deposition faces. In addition, taking both the energy and entropy into account, Bandaru et al. proposed a mechanism whereby for a given volume of material, the helical form occupies the least amount of space and the entropy of the ambient conditions should increase to compensate for the close packing of the helices, which in turn is facilitated by nonwetting catalyst particles or induced by catalyst/ambient agitation in the CVD growth [156].

4.2   Structural models and thermodynamic stabilities

A coiled CNT has a special three-dimensional spiral structure. An important feature is incorporation of pentagons and heptagons in the hexagonal network. Dunlap [51, 157] showed that connecting two CNTs with pentagons and heptagons could result in a kink or knee structure. Based on the knee structure, Fonseca

Figure 9   Experimental fabrication of various kinds of coiled CNTs. Reproduced with permission from Ref. [38]. Copyright 2011 Elsevier.

et al. were able to construct toroidal and coiled CNTs using the knee segments as building blocks, where the former is an in-plane zero-dimensional structure and the latter is an out-of-plane one-dimensional structure [158]. In addition, through cutting the toroidal CNTs into small pieces and recombining them, coiled CNTs with one pitch containing one nanotorus can be constructed [65, 159]. For the coiled CNTs built from toroidal segments, Setton et al. suggested that the toroidal segments were only feasible for single-shell or at most two-shell nanocoils [160]. Another way is to insert pentagons and heptagons into a perfect graphene network and then roll up this structure to form a carbon nanocoil [161, 162]. Similarly, Biró et al. proposed to build the coiled CNTs from rolling up the Haeckelite structure, a graphite sheet composed of polygonal rings [163]. Recently, carbon nanocoils were also constructed from segments of CNTs in which the tube chirality is maintained [164]. Through introducing a pair of pentagons in the outer side and another pair of heptagons in the inner side into the segment of an armchair CNT, a curved structure can be obtained. Using this curved structure as a building block, a carbon nanocoil can be formed by connecting the building blocks with a rotated angle. This method was also employed to construct the structural models of the toroidal CNTs and Z-CNTs, as mentioned

above [39, 61, 111]. A simple schematic diagram of this method is presented in Fig. 10. Usually, a carbon nanocoil can be expressed by the parameters of inner coil diameter D_i, outer coil diameter (D_o), tubular diameter D_t and coil pitch λ [35, 38], as illustrated in Fig. 11.

In addition to the structural models of the coiled CNTs, several studies have been devoted to investigating their thermodynamic stabilities. Comparing the cohesive energies, the coiled CNTs are found to be more stable than the C_{60} fullerene. Employing MD simulations, Ihara et al. [159] obtained cohesive energies of 7.41, 7.39 and 7.43 eV per atom for C_{360}, C_{540} and C_{1080} nanocoils, respectively, which are close to that of a graphite sheet (7.44 eV/atom) and lower than that of the C_{60} fullerene (7.29 eV/atom). Moreover, these carbon nanocoils can maintain the coiled geometry without collapse at temperature up to 1,500 K, which further confirms their thermodynamic stability. Using molecular mechanical (MM) calculations, Feng and Liew studied the structural stability of both armchair and zigzag carbon nanocoils [165]. They found that there is a critical radius beyond which the carbon nanocoil is considered to be stable. If the coil radius is less than the critical radius, stability of the carbon nanocoil is determined by its rising angle. By taking into account the volume free energy, the surface energy,
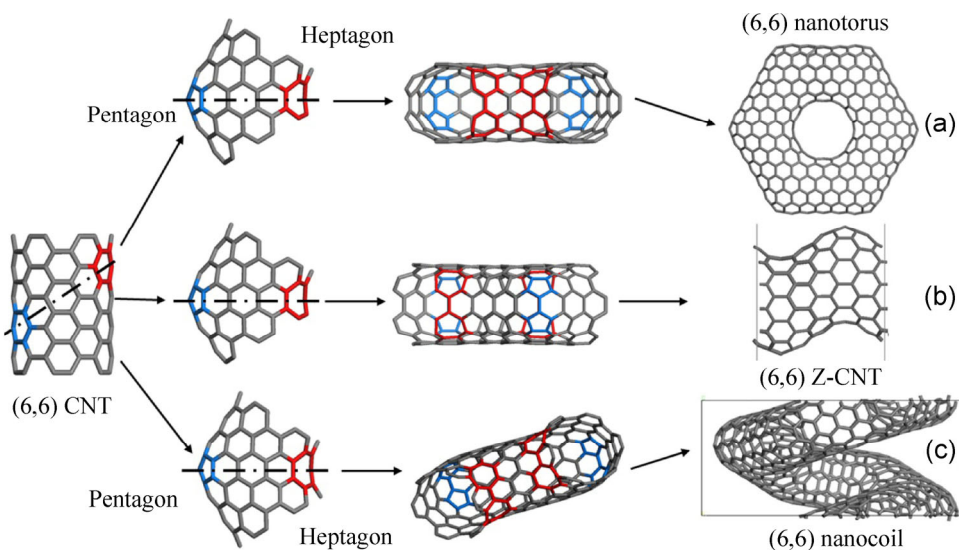

Figure 10 Schematic diagram for constructing the structural models of a (6, 6) carbon nanotorus, Z-CNT, and a nanocoil by introducing pairs of pentagons (highlighted in blue) and heptagons (highlighted in red). (a) is reproduced with permission from Ref. [61]. Copyright 2011 Elsevier. (b) is reproduced with permission from Ref. [111]. Copyright 2013 Royal Society of Chemistry. (c) is reproduced with permission from Ref. [164]. Copyright 2010 Science China Press and Springer-Verlag Berlin Heidelberg.
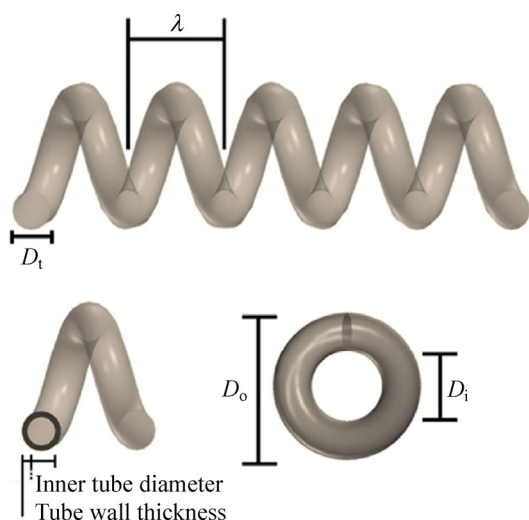
Figure 11 Parameters of inner coil diameter D_i, outer coil diameter D_o, tubular diameter D_t and coil pitch λ to describe a carbon nanocoil. Reproduced with permission from Ref. [38]. Copyright 2011 Elsevier.

and the bending elastic energy due to curvature, it was found that there is a threshold relation between the inner and outer radii for the formation of straight multi-walled CNTs [166], which defines a parameter space where the straight multi-walled CNTs become unstable and undergo a shape deformation to form the coiled CNTs. A recent study shows that the coiled CNTs become more stable as the D_t increases [167]. For a carbon nanocoil, the least stable covalent bonds are located at the pentagon rings on the outer portions of the coils, while the atoms associated with the heptagons in the inner ridge are the most stable. Furthermore, increase in the coil diameters leads to enhanced stability of the covalent bonds [167].

4.3 Mechanical properties

It is well-known that a spring can be easily stretched or compressed by a large elastic strain, which is very useful in mechanical devices. Since the carbon nanocoil has similar spiral geometry to a spring, many studies have been carried out to investigate mechanical properties of the coiled CNTs. In 2,000, using an AFM, Volodin et al. measured the elastic properties of the coiled CNTs and found that the coiled CNTs with coil diameters (>170 nm) possess high Young's modulus (E) of 0.4–0.9 TPa [168]. However, much smaller E of 0.04–0.13 TPa and elastic spring constants of

0.01–0.6 N/m for the coiled CNTs with coil diameters ranging from 144 to 830 nm were predicted by Hayashida et al. from a manipulator-equipped SEM measurement [169]. In particular, remarkable spring-like behavior of an individual carbon nanocoil has been demonstrated by Chen et al. [170], as presented in Fig. 12. A spring constant of 0.12 N/m in the low-strain regime and a maximum elastic elongation of 33% were obtained from the AFM measurements. In contrast to the high value of E, the shear modulus (G) of the coiled CNTs is extremely low. Chen et al. [170] reported coiled CNTs with a D_o of ~126 nm ± 4 nm but different D_i. For $D_i = 3/4$ D_o, a G of ~2.5 GPa ± 0.4 GPa was obtained; for $D_i = 1/2$ D_o, the G was ~2.3 GPa ± 0.4 GPa; for $D_i = 0$, the G was ~2.1 GPa ± 0.3 GPa. Huang [171] studied coiled CNTs under uniaxial tension in simple explicit expressions and obtained a maximum elastic elongation of ~30%, a G of 2.8–3.4 GPa and a spring constant of ~0.1–0.4 N/m for the double nanocoils formed by twisting two single nanocoils, values which are comparable to experimental results [170]. Chang et al. reported a G of 3 GPa ± 0.2 GPa for the double coiled CNTs [172]. Generally, the value of G for carbon nanocoils is only a few GPa, while the value of E can be hundreds of GPa. In addition, reversibility of the coiled CNTs under strain is a useful feature. Chen et al. found that the coiled CNT can be elastically loaded to a relative elongation of 33% and return completely
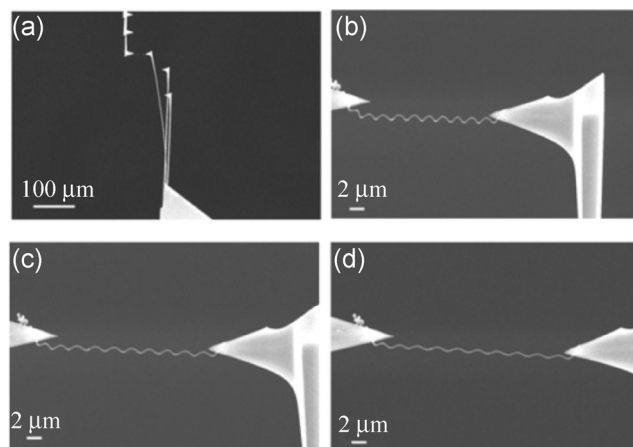

Figure 12 Measurement of the mechanical properties of a carbon nanocoil using AFM cantilevers: (b) the initial state, (c) at a tensile strain of 20%, and (d) at a tensile strain of 33%. Reproduced with permission from Ref. [170]. Copyright 2003 American Chemical Society.

to the equilibrium geometry without apparent plastic deformation [170]. Another study carried out by Poggi et al. considering the compression behavior of the coiled CNTs demonstrated that repeated compression/buckling/decompression of the carbon nanocoil was very reproducible with a limiting compression of 400 nm [173].

Theoretical studies of the mechanical properties of coiled CNTs were also carried out to further understand the experimental measurements. Using the Kirchhoff rod model, Fonseca et al. derived a series of expressions to obtain E and Poisson's ratio for the coiled CNTs. Taking the parameters for the carbon nanocoils reported by Chen et al. [170], Fonseca et al. estimated E to be 6.88 GPa, with a Poisson's ratio of 0.27 and a value of G of 2.5 GPa for a carbon nanocoil with D_t = 120 nm, D_o = 840 nm and λ = 2,000 nm [174, 175]. The E and elastic constant of a series of nanocoils built from the armchair SWNTs were calculated by Liu et al., employing DFT and TB methods [164]. They showed that the E of carbon nanocoils ranges from 3.43 to 5.40 GPa, in good agreement with Fonseca's results [174, 175] and the elastic constant lies between 15.37 and 44.36 N/m, higher than the experimental values [168, 170]. Furthermore, superelastic behavior of the coiled CNTs was predicted [164], where the coiled CNTs can undertake an elastically tensile strain up to ~60% and compressive strain up to ~20%–35%. Such superelasticity is due to the invariance of bond length under strain associated with the strong covalent C–C bonding, indicating excellent reversibility of coiled CNTs as reported in experiments [170, 173]. Using the MD finite element method, Ghaderi and Hajiesmaili also reported the superelasticity of coiled CNTs under tension with a fracture strain in the range of 50% and 66% [176]. For coiled CNTs built from (n, n) CNTs with n = 5–18, the spring constant increases with the tubular diameter D_t, ranging from 15 to 30 N/m [176, 177]. Using the MD simulations with the LAMMPS package and the adaptive intermolecular reactive empirical bond-order potential, Wu et al. investigated the stretching instability and reversibility of tightly wound coiled CNTs [167]. It was found that the coiled CNTs exhibit extensive stretching ability in the range from 400% to 1,000%, as a result of two distinct deformation mechanisms depending on the nanocoil size, as presented in Fig. 13. For small nanocoils, tremendous deformation is achieved by domino-type partial fracture events, whereas for large nanocoils it is accomplished by stepwise buckling of coils. On the other hand, a study of the elastic constants of coiled CNT forests showed that the entanglement among neighboring nanocoils due to the bending of the coil tips produced by the ball impact will contribute to the mechanical properties of the nanocoil forests and lead to a nonlinear elastic behavior [178]. Generally speaking, the calculated E and elastic constants for the coiled CNTs are different, to a greater or lesser, from the experimental values. This difference may be attributed to the structural details of the synthesized carbon nanocoils, especially the larger sizes of experimental nanocoil samples.

4.4 Electronic and transport properties

Due to the presence of pentagons and heptagons in the coiled CNTs, they exhibit different electric properties from those of the pristine CNTs. In 1996, Kaneto et al. measured the electric conductivity of the carbon microcoils using two and four probe methods, and found values in the range 30–100 S/cm [179]. Shen et al. found that the electric conductivity of single carbon microcoils is about 120 S/cm at room temperature [180]. The resistance of carbon microcoils is temperature-dependent, and increases rapidly with decreasing temperature. The temperature dependence of the electrical resistance was also observed in Fujii et al.'s work where the resistivity of the carbon nanocoil was found to decrease as the annealing temperature increases [181]. In addition, Hayashida et al. found that for a carbon nanocoil with a coil diameter of 196 nm and a length of 1.5 mm, the conductivity is about 180 S/cm [169], which is much smaller than a straight CNT (~10^4 S/cm) [182]. Recently, Chiu et al. reported a very high conductivity of 2,500 S/cm and an electron hopping length of ~5 nm for single carbon nanocoils measured at low temperature [183]. An even higher electron hopping length of 5–50 nm was predicted by Tang et al. [184]. Generally, the measured electric properties of the coiled CNTs depend strongly on temperature and details of sample. Table 2 summarizes the electronic properties of the coiled CNTs reported in literature.
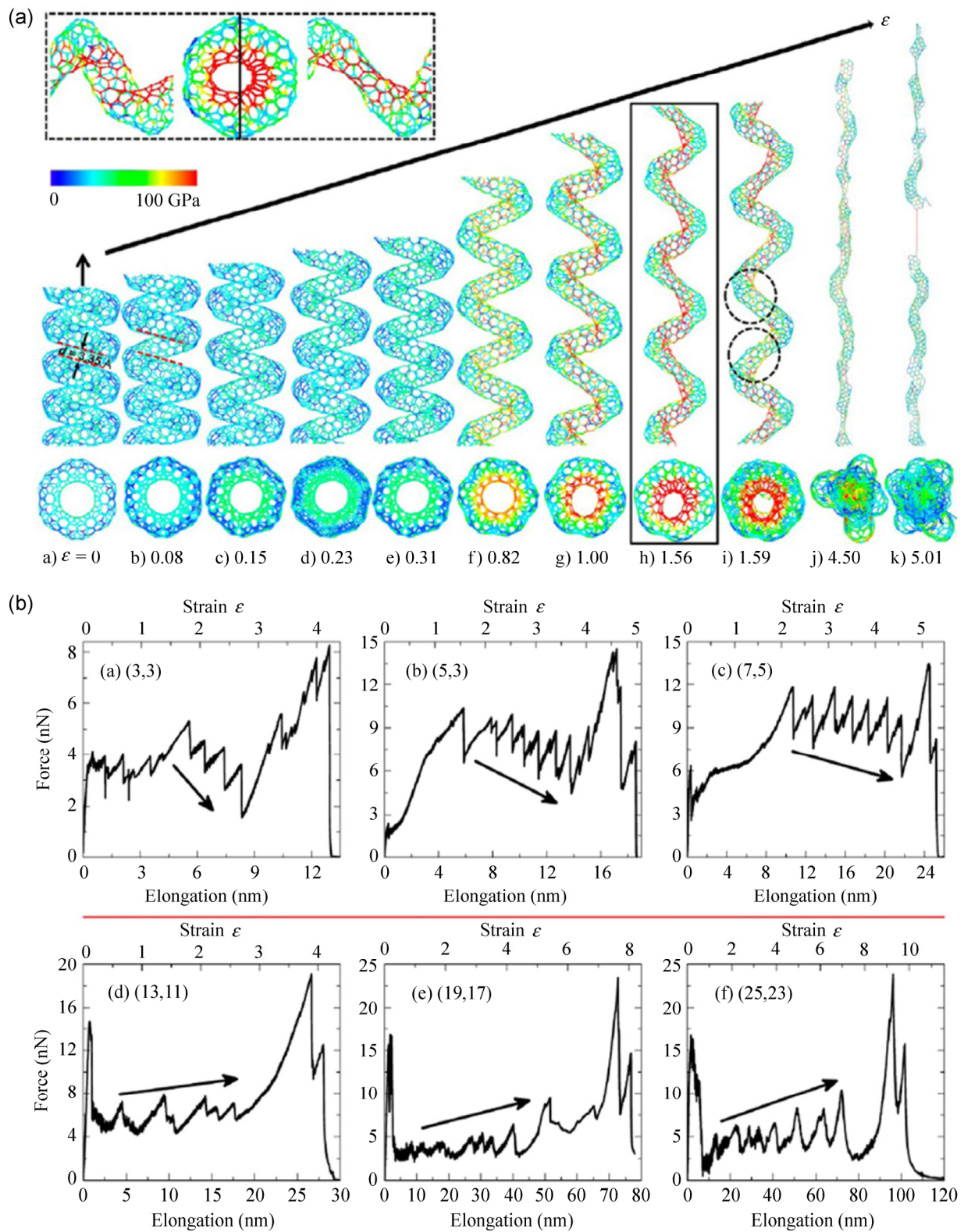
Figure 13 Mechanical properties of a carbon nanocoil: (a) atomic structural evolution of the (5, 3) carbon nanocoil during tension loading, (b) tensile force versus elongation (strain) curves of a series of tightly wound carbon nanocoils. Reproduced with permission from Ref. [167]. Copyright 2013 American Chemical Society.

Table 2 Parameters to characterize the electronic properties of the coiled CNTs. T_M is the characteristic Mott temperature, T_{ES} is the characteristic Efros−Shklovskii temperature, $N(E_F)$ is the density of states at the Fermi energy E_F, l is the localization length and κ is the dielectric constant, respectively. Some of the values are reproduced with permission from Ref. [184]. Copyright 2010 American Chemical Society

Sample description	Ref. [169]	Ref. [179]	Ref. [180]	Ref. [183]	Ref. [184]
coil diameter (nm)	180−350	~5,000	~2,000	~150	~150
coil length (μm)	~1.5	~2,000	~2,500	~5	~30
T_M (K)	N/A	N/A	2,342	N/A	215
T_{ES} (K)	N/A	N/A	17.5	0.17	272
$N(E_F)$ (eV^{-1}·cm^{-3})	N/A	N/A	~10^{19}	4.4×10^{20}	N/A
L (nm)	N/A	N/A	13.2	32	11–50
κ	N/A	N/A	~10^3	~10^6	50–200
Coulomb gap (MeV)	N/A	N/A	0.12	1.5×10^{-3}	23.8
conductivity (S·cm^{-1})	100–180	30–100	120	~25	N/A

Several theoretical studies have also been carried out to explore the electronic properties of the coiled CNTs. Employing a simple TB model, Akagi et al. [161, 162] calculated the band structures and electron density of states of carbon nanocoils and suggested that the coiled CNTs could be metallic, semiconducting or semimetallic, depending on the arrangement of the pentagons and heptagons. Since the pristine CNTs can only be either metallic or semiconducting, the existence of a semimetal is unique for the carbon nanocoils [162]. Using a π-orbital TB model combined with the Green's function approach, Liu et al. investigated the electrical conductance of a series of carbon nanocoils built from armchair CNTs [185]. By employing the metallic armchair CNT segments as electrodes, quantum conductance of the (5, 5), (6, 6) and (7, 7) carbon nanocoils were calculated, as presented in Fig. 14. Clearly, there is a transport gap in the conductance spectrum. Further analysis of the electronic states indicated that the incorporation of pentagons and heptagons (such as Stone–Wales defects) alone cannot lead to gap opening; thus creation of the band gap is attributed to the existence of sp^3 C–C bonds caused by coiling the CNTs. The sp^3 hybridization C–C bonds can make electrons localized and open a transport gap, similar to the squashed CNTs [116]. In addition, no significant change of quantum conductance was found for carbon nanocoils under uniaxial elongation or compression due to the nearly invariant bond length under strain, i.e., superelasticity [164].

4.5 Chemical properties

The helical structure of the coiled CNT makes it a good catalytic support. It was found that PtRu alloy nanoparticles grown on the coiled CNT exhibit excellent crystallinity and a large surface area, leading
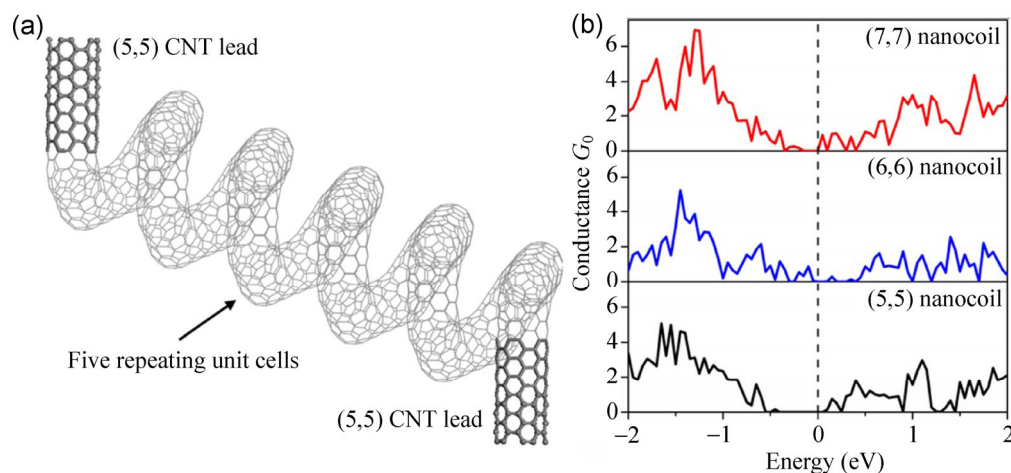

Figure 14 Structural model to calculate the conductance of a (5, 5) carbon nanocoil (a) and the conductance of (5, 5), (6, 6) and (7, 7) carbon nanocoils (b). Reproduced with permission from Ref. [185]. Copyright (2011) by Science China Press and Springer-Verlag Berlin Heidelberg.

to excellent catalytic activity [152]. This suggests the coiled CNT be a promising candidate for fuel cell applications, offering the potential advantages of a considerable reduction in the amount of catalyst, acceleration of diffusion of methanol fuel, and removal of by-product CO_2 gas. The excellent performance of the coiled CNT-supported catalyst in an electrochemical cell can be attributed to the superior dispersion of nanosized metallic nanoparticles on the coiled CNT and the good interaction between the support material and the metal catalyst particles. In addition, due to the large curvature, it is energetically preferable for nitrogen to be doped into the coiled CNTs with a high doping concentration of ~3.5% [186]. A fuel cell using the nitrogen-doped coiled CNTs showed an improved performance over the one using the undoped coiled CNTs [187]. Through changing the annealing temperature during synthesis of the nitrogen-doped coiled CNTs via CVD, the nitrogen doping concentration, doping type, and the resulting optical properties can all be manipulated [188]. Furthermore, the coiled CNTs can be combined with polymer materials and used in electrochemical cells [189].

4.6 Field emission and electromagnetic wave absorption

It is well-known that CNTs can serve as field emission devices due to their sharp tips [190, 191]. Compared with CNTs, the coiled CNTs not only have tips but also possess curved edges along the body due to the existence of defective rings (pentagons and heptagons) and buckling. Therefore, the coiled CNTs may also be good candidates for field emission devices. In 2003, Jiao et al. [192] found that similar to CNTs, coiled CNTs can emit electrons and photons in the presence of a sufficiently strong electric field and the field-emission current density obtained from the coiled CNTs was on the order of 10^4 A·cm^{-2}, comparable to the values commonly seen in metal emitters. This suggests that carbon coils are good candidates for field emission applications. Particularly, non-linear emission resulting in Fowler–Nordheim (FN) plots was observed in some coiled CNTs [193]. Using a phosphorus glass plate coated with indium tin oxide as the anode and an iron needle coated with aligned coiled CNTs acts as the cathode, Zhang et al. [149] showed a rather low

turn-on electrical field and high current for the field emission of carbon nanocoils. Features of FN plots were also observed, which might be due to the large number of emission sites formed by the tips and edges of the carbon nanocoils. Later, Hokushin et al. confirmed Zhang's explanation that both the tips and edges of the carbon nanocoils can serve as emitters [194]. They found that for a carbon nanocoil, the emission spot consists of two parts: one is from the tip of the nanocoil and the other is from the side body of the top surface, as presented in Fig. 15. In addition, there is a structural change in the carbon nanocoil during field emission, as shown in Fig. 15, which is considered to be induced by the Joule heating associated with the large emission current. On the other hand, the field emission of carbon nanocoils can be enhanced by some treatments. It was found that the field emission of carbon nanocoils is uniformly enhanced after an electrical discharge machining process [195]. Also, through a simple thermal CVD process, the coiled CNTs show very low turn-on field, high emission current and very good resistance to degradation with time. These enhanced field emission properties can be explained from the point of view of material selection and structures of the CNTs [196].
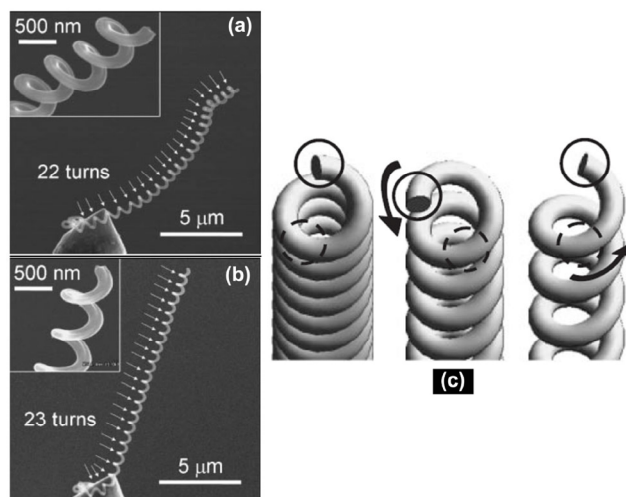

Figure 15   Field emission properties of carbon nanocoils: (a) SEM image of the carbon nanocoil before field emission; (b) SEM image of the carbon nanocoil after field emission; and (c) field emission sites of the carbon nanocoil, where solid circles indicate the tip of the nanocoil and dashed circles indicate the side body of the top surface. Reproduced with permission from Ref. [194]. Copyright 2007 The Japan Society of Applied Physics.

In addition to field emission, the coiled CNTs can also absorb electromagnetic waves. Tang et al. found that the plait-like coiled CNTs present good microwave absorbing ability, especially in the high-frequency range [197]. With a matching thickness of 1.8 mm, the maximum reflection loss is ca. –20 dB and the bandwidth corresponding to the reflection loss below –10 dB is more than 4.31 GHz. The bandwidth of the plait-like coiled CNTs is wider than that of SWNTs/ soluble cross-linked polyurethane composites under high loading [198]. Similarly, for twin-coiled CNTs, the maximum reflection loss and bandwidth corresponding to reflection loss below –10 dB are –36.09 dB and 6.43 GHz, respectively, suggesting superior microwave absorption to the plait-like coiled CNTs [199]. Furthermore, the coiled CNTs show more efficient photoluminescence than their multi-walled CNT counterparts due to a large surface-to-volume ratio and abundant electrons on its surfaces [200]. Wen et al. also found that after doping with nitrogen atoms, there was a strong ultraviolet photoluminescence emission from the carbon nanocoils [188]. The light emission of single coiled CNTs in the wavelength range from 600 to 900 nm induced by photo and thermal excitations was also reported by Ma et al. [201], as well as a near-infrared response with a maximum responsivity of 0.22 A/W [202].

4.7 Applications

Since coiled CNTs possess special spiral structures and excellent mechanical and electronic properties, they have potential applications in various fields complementary to their straight counterparts [35, 38, 140, 203]. One important application for carbon nanocoils is to act as sensors. In 2004, Volodin et al. [204] reported the use of coiled nanotubes as self-sensing mechanical resonators, which are able to detect fundamental resonances ranging from 100 to 400 MHz, as illustrated in Fig. 16. The self-sensing carbon nanocoil sensors are sensitive to mass change and well suited for measuring small forces and masses in the femtogram range. After measuring the mechanical response of the coiled CNTs under compression using AFM, Poggi et al. pointed out that a nonlinear response of the carbon nanocoil can be observed, which is associated with compression and buckling of the nanocoil [173]. Bell et al. demonstrated that the coiled CNTs can be used as high-resolution force sensors in conjunction with visual displacement measurement as well as electromechanical sensors due to the piezoresistive behavior without an additional metal layer [205]. The applications of carbon nanocoils as near-infrared sensors [201], magnetic sensors [206], tactile sensors [207] and gas sensors [208] were also explored.

Another application for carbon nanocoils is to form composites with other materials, which can enhance their properties. By adding carbon nanocoils into epoxy nanocomposites, their mechanical properties can be enhanced [209–212]. Coiled CNT/silicone-rubber composites show high resistive sensitivity, depending on the density of carbon nanocoils [213, 214]. In addition, coiled CNTs coated with Ni show enhanced microwave absorption compared with the uncoated ones, resulting from stronger dielectric and magnetic losses [215]. Tungsten-containing carbon nanocoils can expand and contract as flexibly as macro-scale springs and the elastic constants of the tungsten-containing carbon nanocoils increases with increasing
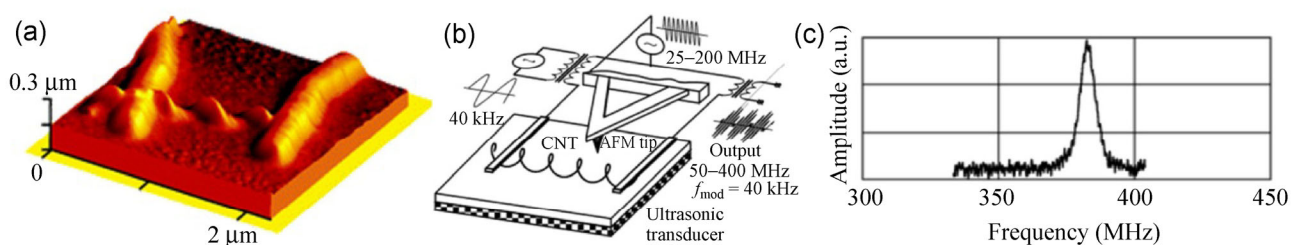

Figure 16 Carbon nanocoil acting as a mechanical resonator: (a) AFM image of the carbon nanocoil; (b) the circuit containing two broad-band radio frequency transformers and the carbon nanocoil; (c) resonant response of the carbon nanocoil device to electromechanical excitation. Reproduced with permission from Ref. [204]. Copyright 2004 American Chemical Society.

concentration of tungsten [216]. In addition, coiled CNT composites have been utilized as energy storage devices, such as fuel cells [151], lithium-ion batteries [217], and electrochemical devices [189, 218, 219]. Moreover, coiled CNTs have been used as sensors, flat panel field emission displays, microwave absorbers and additives in the cosmetic industry.

5   Conclusions and outlook

Both experimental and theoretical studies of toroidal, kinked and coiled CNTs have been reviewed, including fabrication and formation mechanisms, theoretical modelling, physical and chemical properties, and technological applications. Compared with pristine CNTs, zero-dimensional toroidal CNTs exhibit better electromagnetic properties, such as persistent current and an Aharonov–Bohm effect. Moreover, the electronic properties of the toroidal CNTs can be tuned by chemical modification. In particular, this tubular closed structure can trap ions, atoms and molecules. In contrast to toroidal CNTs, kinked and coiled CNTs are kinds of spiral structures. The former are in-plane spirals and the latter are out-of-plane spirals. The kinked CNTs have enhanced chemical reactivity at the kinked parts and can be promising candidates for nanoscale sensors and switches due to the significant electromechanical coupling effects. On the other hand, the coiled CNTs possess fascinating mechanical, optical, chemical and field emission properties. In addition, the superior mechanical properties allow the coiled CNTs to act as electromechanical, electromagnetic, and chemical sensors.

As mentioned above, the toroidal CNTs synthesized experimentally are usually formed by bundles of SWNTs and have large tubular diameters. The fabrication of single-walled toroidal CNTs, as well as toroidal CNTs with controllable tubular diameters, remains a great challenge. Inserting atoms/molecules into the toroidal CNTs is an interesting topic of future study. Similar to the toroidal CNTs, experimentally fabricated kinked CNTs are composed of bundle of SWNTs and it is hard to control the geometries and bending angles. Thus, improved experimental techniques and parameters affording kinked CNTs

with controllable wall thickness and geometry should be developed. On the other hand, both experimental and theoretical studies are needed to further explore their properties for potential applications. In addition, since the formation mechanism of the coiled CNTs depends strongly on the catalyst, searching for the optimal catalysts is critical for improving quality and quantity of the nanocoil samples. Finding the appropriate geometry and concentration of the coiled CNTs is necessary to improve performance of nanocoil-based nanocomposites. To realize applications in nanodevices, it is also important to elucidate the contact interaction between these carbon nanostructures with electrodes or other coating materials.

Inspired by the extensive research on CNTs and graphene, low-dimensional non-carbon nanostructures (one-dimensional and two-dimensional) have also attracted great attention, such as nanotubes of BN, vanadium oxide, chalcogenides, bismuth, and $NiCl_2$ [220–223], nanoribbons of BN [224], MX_2 [225–227], GaN [228], molybdite [229], and selenium [230], two-dimensional monolayera of BN [231, 232], MX_2 [233–235], silicone [236–241], and the recently proposed and fabricated organic topological insulators made of two-dimensional organometallic frameworks [242–245]. It would be interesting to extend the study of kinked and coiled CNT to non-carbon counterparts, for example, kinked BN [246, 247] and semiconductor nanowires/nanotubes [248–251], kinked inorganic nanoribbons [129], and coiled BN [252], ZnO [253], and silica [254] nanotubes.

Acknowledgements

References

[1] Ichihashi, T.; Ando, Y. Pentagons, heptagons and negative curvature in graphite microtubule growth. *Nature* **1992**, *356*, 776–778.

[2] Ball, P. Needles in a carbon haystack. *Nature* **1991**, *354*, 18.

[3] Charlier, J. C. Defects in carbon nanotubes. *Acc. Chem. Res.* **2002,** *35*, 1063–1069.

[4] Liu, J.; Dai, H. J.; Hafner, J. H.; Colbert, D. T.; Smalley, R. E.; Tans, S. J.; Dekker, C. Fullerene "crop circles". *Nature* **1997**, *385*, 780–781.

[5] Falvo, M.; Clary, G.; Taylor, R.; Chi, V.; Brooks, F.; Washburn, S.; Superfine, R. Bending and buckling of carbon nanotubes under large strain. *Nature* **1997**, *389*, 582–584.

[6] Yao, Z.; Postma, H. W. C.; Balents, L.; Dekker, C. Carbon nanotube intramolecular junctions. *Nature* **1999**, *402*, 273–276.

[7] Terrones, M.; Terrones, H.; Banhart, F.; Charlier, J. C.; Ajayan, P. M. Coalescence of single-walled carbon nanotubes. *Science* **2000**, *288*, 1226–1229.

[8] Amelinckx, S.; Zhang, X. B.; Bernaerts, D.; Zhang, X. F.; Ivanov, V.; Nagy, J. B. A formation mechanism for catalytically grown helix-shaped graphite nanotubes. *Science* **1994**, *265*, 635–639.

[9] Zhang, X. B.; Zhang, X. F.; Bernaerts, D.; van Tendeloo, G.; Amelinckx, S.; van Landuyt, J.; Ivanov, V.; Nagy, J. B.; Ph, L.; Lucas, A. A. The texture of catalytically grown coil-shaped carbon nanotubules. *Europhys. Lett.* **1994**, *27*, 141–146.

[10] Martel, R.; Shea, H. R.; Avouris, P. Rings of single-walled carbon nanotubes. *Nature* **1999**, *398*, 299.

[11] Martel, R.; Shea, H. R.; Avouris, P. Ring formation in single-wall carbon nanotubes. *J. Phys. Chem. B* **1999**, *103*, 7551–7556.

[12] Sano, M.; Kamino, A.; Okamura, J.; Shinkai, S. Ring closure of carbon nanotubes. *Science* **2001**, *293*, 1299–1301.

[13] Geng, J.; Ko, Y. K.; Youn, S. C.; Kim, Y.-H.; Kim, S. A.; Jung, D.-H.; Jung, H.-T. Synthesis of SWNT rings by noncovalent hybridization of porphyrins and single-walled carbon nanotubes. *J. Phys. Chem. C* **2008**, *112*, 12264–12271.

[14] Song, L.; Ci, L. J.; Sun, L. F.; Jin, C.; Liu, L.; Ma, W.; Liu, D.; Zhao, X.; Luo, S.; Zhang, Z.; et al. Large-scale synthesis of rings of bundled single-walled carbon nanotubes by floating chemical vapor deposition. *Adv. Mater.* **2006**, *18*, 1817–1821.

[15] Zhou, Z.; Wan, D.; Bai, Y.; Dou, X.; Song, L.; Zhou, W.; Mo, Y.; Xie, S. Ring formation from the direct floating catalytic chemical vapor deposition. *Physica E* **2006**, *33*, 24–27.

[16] AuBuchon, J. F.; Chen, L.-H.; Gapin, A. I.; Kim, D.-W.; Daraio, C.; Jin, S. Multiple sharp bendings of carbon nanotubes during growth to produce zigzag morphology. *Nano Lett.* **2004**, *4*, 1781–1784.

[17] AuBuchon, J. F.; Chen, L.-H.; Jin, S. Control of carbon capping for regrowth of aligned carbon nanotubes. *J. Phys. Chem. B* **2005**, *109*, 6044–6048.

[18] Hertel, T.; Martel, R.; Avouris, P. Manipulation of individual carbon nanotubes and their interaction with surfaces. *J. Phys. Chem. B* **1998**, *102*, 910–915.

[19] Postma, H. W. C.; Teepen, T.; Yao, Z.; Grifoni, M.; Dekker, C. Carbon nanotube single-electron transistors at room temperature. *Science* **2001**, *293*, 76–79.

[20] Gao, R.; Wang, Z. L.; Fan, S. Kinetically controlled growth of helical and zigzag shapes of carbon nanotubes. *J. Phys. Chem. B* **2000**, *104*, 1227–1234.

[21] Ismach, A.; Segev, L.; Wachtel, E.; Joselevich, E. Atomic-step-templated formation of single wall carbon nanotube patterns. *Angew. Chem. Int. Edit.* **2004**, *43*, 6140–6143.

[22] Pan, L.; Hayashida, T.; Zhang, M.; Nakayama, Y. Field emission properties of carbon tubule nanocoils. *Jpn. J. Appl. Phys.* **2001**, *40*, L235–L237.

[23] Xie, J.; Mukhopadyay, K.; Yadev, J.; Varadan, V. Catalytic chemical vapor deposition synthesis and electron microscopy observation of coiled carbon nanotubes. *Smart Mater. Struct.* **2003**, *12*, 744–748.

[24] Hou, H.; Jun, Z.; Weller, F.; Greiner, A. Large-scale synthesis and characterization of helically coiled carbon nanotubes by use of $Fe(CO)_5$ as floating catalyst precursor. *Chem. Mater.* **2003**, *15*, 3170–3175.

[25] Zhong, D. Y.; Liu, S.; Wang, E. G. Patterned growth of coiled carbon nanotubes by a template-assisted technique. *Appl. Phys. Lett.* **2003**, *83*, 4423–4425.

[26] Tang, N.; Wen, J.; Zhang, Y.; Liu, F.; Lin, K.; Du, Y. Helical carbon nanotubes: Catalytic particle size-dependent growth and magnetic properties. *ACS Nano* **2010**, *4*, 241–250.

[27] Thostenson, E. T.; Ren, Z.; Chou, T.-W. Advances in the science and technology of carbon nanotubes and their composites: A review. *Compos. Sci. Technol.* **2001**, *61*, 1899–1912.

[28] Lin, Y.; Taylor, S.; Li, H.; Fernando, K. A. S.; Qu, L.; Wang, W.; Gu, L.; Zhou, B.; Sun, Y.-P. Advances toward bioapplications of carbon nanotubes. *J. Mater. Chem.* **2004**, *14*, 527–541.

[29] Britz, D. A.; Khlobystov, A. N. Noncovalent interactions of molecules with single walled carbon nanotubes. *Chem. Soc. Rev.* **2006**, *35*, 637–659.

[30] Singh, P.; Campidelli, S.; Giordani, S.; Bonifazi, D.; Bianco, A.; Prato, M. Organic functionalisation and characterisation of single-walled carbon nanotubes. *Chem. Soc. Rev.* **2009**, *38*, 2214–2230.

[31] Dresselhaus, M. S.; Dresselhaus, G.; Eklund, P. C. *Science of Fullerenes and Carbon Nanotubes: Their Properties and Applications*; Academic Press: Waltham, 1996.

[32] Ebbesen, T. W. *Carbon Nanotubes: Preparation and Properties*; CRC press: Boca Raton, 1997.

[33] Saito, R.; Dresselhaus, G.; Dresselhaus, M. S. *Physical Properties of Carbon Nanotubes*; Imperial College Press: London, 1998.

[34] Reich, S.; Thomsen, C.; Maultzsch, J. *Carbon Nanotubes*; John Wiley & Sons: Hoboken, 2008.

[35] Lau, K. T.; Lu, M.; Hui, D. Coiled carbon nanotubes: Synthesis and their potential applications in advanced composite structures. *Compos. Part B: Eng.* **2006**, *37*, 437–448.

[36] Fejes, D.; Hernádi, K. A review of the properties and CVD synthesis of coiled carbon nanotubes. *Materials* **2010**, *3*, 2618–2642.

[37] Hanus, M. J.; Harris, A. T. Synthesis, characterisation and applications of coiled carbon nanotubes. *J. Nanosci. Nanotechnol.* **2010**, *10*, 2261–2283.

[38] Shaikjee, A.; Coville, N. J. The synthesis, properties and uses of carbon materials with helical morphology. *J. Adv. Res.* **2012**, *3*, 195–223.

[39] Liu, L.; Zhao, J. Toroidal and coiled carbon nanotubes. In *Syntheses and Applications of Carbon Nanotubes and Their Composites*; Suzuki, S., Ed.; InTech: Croatia, 2013; pp. 257–282.

[40] Ahlskog, M.; Seynaeve, E.; Vullers, R. J. M.; Van Haesendonck, C.; Fonseca, A.; Hernadi, K.; Nagy, J. B. Ring formations from catalytically synthesized carbon nanotubes. *Chem. Phys. Lett.* **1999**, *300*, 202–206.

[41] Wang, Y.; Maspoch, D.; Zou, S.; Schatz, G. C.; Smalley, R. E.; Mirkin, C. A. Controlling the shape, orientation, and linkage of carbon nanotube features with nano affinity templates. *Proc. Natl. Acad. Sci. U. S. A.* **2006**, *103*, 2026–2031.

[42] Kukushkin, A. B.; Neverov, V. S.; Marusov, N. L.; Semenov, I. B.; Kolbasov, B. N.; Voloshinov, V. V.; Afanasiev, A. P.; Tarasov, A. S.; Stankevich, V. G.; Svechnikov, N. Y.; et al. Few-nanometer-wide carbon toroids in the hydrocarbon films deposited in tokamak T-10. *Chem. Phys. Lett.* **2011**, *506*, 265–268.

[43] Wang, X.; Wang, Z.; Liu, Y. Q.; Wang, C.; Bai, C.; Zhu, D. Ring formation and fracture of a carbon nanotube. *Chem. Phys. Lett.* **2001**, *339*, 36–40.

[44] Lyn, M. E.; He, J.; Koplitz, B. Laser-induced production of large carbon-based toroids. *Appl. Surf. Sci.* **2005**, *246*, 44–47.

[45] Motavas, S.; Omrane, B.; Papadopoulos, C. Large-area patterning of carbon nanotube ring arrays. *Langmuir* **2009**, *25*, 4655–4658.

[46] Chen, L.; Wang, H.; Xu, J.; Shen, X.; Yao, L.; Zhu, L.; Zeng, Z.; Zhang, H.; Chen, H. Controlling reversible elastic deformation of carbon nanotube rings. *J. Am. Chem. Soc.* **2011**, *133*, 9654–9657.

[47] Komatsu, N.; Shimawaki, T.; Aonuma, S.; Kimura, T. Ultrasonic isolation of toroidal aggregates of single-walled carbon nanotubes. *Carbon* **2006**, *44*, 2091–2093.

[48] Guo, A.; Fu, Y.; Guan, L.; Zhang, Z.; Wu, W.; Chen, J.; Shi, Z.; Gu, Z.; Huang, R.; Zhang, X. Spontaneously formed closed rings of single-wall carbon nanotube bundles and their physical mechanism. *J. Phys. Chem. C* **2007**, *111*, 3555–3559.

[49] Colomer, J. F.; Henrard, L.; Flahaut, E.; Van Tendeloo, G.; Lucas, A. A.; Lambin, P. Rings of double-walled carbon nanotube bundles. *Nano Lett.* **2003**, *3*, 685–689.

[50] Yu, H.; Zhang, Q.; Luo, G.; Wei, F. Rings of triple-walled carbon nanotube bundles. *Appl. Phys. Lett.* **2006**, *89*, 223106.

[51] Dunlap, B. I. Connecting carbon tubules. *Phys. Rev. B* **1992**, *46*, 1933–1936.

[52] Itoh, S.; Ihara, S.; Kitakami, J.-I. Toroidal form of carbon C_{360}. *Phys. Rev. B* **1993**, *47*, 1703–1704.

[53] Ihara, S.; Itoh, S.; Kitakami, J.-I. Toroidal forms of graphitic carbon. *Phys. Rev. B* **1993**, *47*, 12908–12911.

[54] Itoh, S.; Ihara, S. Toroidal forms of graphitic carbon. II. Elongated tori. *Phys. Rev. B* **1993**, *48*, 8323–8328.

[55] Kirby, E. C.; Mallion, R. B.; Pollak, P. Toroidal polyhexes. *J. Chem. Soc., Faraday Trans.* **1993**, *89*, 1945–1953.

[56] Liu, L.; Jayanthi, C. S.; Wu, S. Y. Structural and electronic properties of a carbon nanotorus: Effects of delocalized and localized deformations. *Phys. Rev. B* **2001**, *64*, 033412.

[57] Liu, L.; Guo, G. Y.; Jayanthi, C. S.; Wu, S. Y. Colossal paramagnetic moments in metallic carbon nanotori. *Phys. Rev. Lett.* **2002**, *88*, 217206.

[58] Hod, O.; Rabani, E.; Baer, R. Carbon nanotube closed-ring structures. *Phys. Rev. B* **2003**, *67*, 195408.

[59] Cox, B. J.; Hill, J. M. New carbon molecules in the form of elbow-connected nanotori. *J. Phys. Chem. C* **2007**, *111*, 10855–10860.

[60] Baowan, D.; Cox, B. J.; Hill, J. M. Toroidal molecules formed from three distinct carbon nanotubes. *J. Math. Chem.* **2008**, *44*, 515–527.

[61] Liu, L.; Zhang, L.; Gao, H.; Zhao, J. Structure, energetics, and heteroatom doping of armchair carbon nanotori. *Carbon* **2011**, *49*, 4518–4523.

[62] Itoh, S.; Ihara, S. Isomers of the toroidal forms of graphitic carbon. *Phys. Rev. B* **1994**, *49*, 13970–13974.

[63] Nagy, C.; Nagy, K.; Diudea, M. Elongated tori from armchair DWNT. *J. Math. Chem.* **2009**, *45*, 452–459.

[64] László, I.; Rassat, A. Toroidal and spherical fullerene-like molecules with only pentagonal and heptagonal faces. *Int. J. Quantum Chem.* **2001**, *84*, 136–139.

[65] Ihara, S.; Itoh, S. Helically coiled and toroidal cage forms of graphitic carbon. *Carbon* **1995**, *33*, 931–939.

[66] Taşcı, E.; Yazgan, E.; Malcıoğlu, O. B.; Erkoç, Ş. Stability of carbon nanotori under heat treatment: Molecular-dynamics simulations. *Fullerenes Nanotubes Carbon Nanostruct.* **2005**, *13*, 147–154.

[67] Chen, C.; Chang, J.-G.; Ju, S.-P.; Hwang, C.-C. Thermal stability and morphological variation of carbon nanorings of different radii during the temperature elevating process: A molecular dynamics simulation study. *J. Nanoparticle Res.* **2011**, *13*, 1995–2006.

[68] Yang, L.; Chen, J.; Dong, J. Stability of single-wall carbon nanotube tori. *Physica Status Solidi B* **2004**, *241*, 1269–1273.

[69] Feng, C.; Liew, K. M. Energetics and structures of carbon nanorings. *Carbon* **2009**, *47*, 1664–1669.

[70] Liu, P.; Zhang, Y. W.; Lu, C. Structures and stability of defect-free multiwalled carbon toroidal rings. *J. Appl. Phys.* **2005**, *98*, 113522.

[71] Han, J. Energetics and structures of fullerene crop circles. *Chem. Phys. Lett.* **1998**, *282*, 187–191.

[72] Meunier, V.; Lambin, P.; Lucas, A. A. Atomic and electronic structures of large and small carbon tori. *Phys. Rev. B* **1998**, *57*, 14886–14890.

[73] Chang, I.; Chou, J.-W. A molecular analysis of carbon nanotori formation. *J. Appl. Phys.* **2012**, *112*, 063523.

[74] Chen, N.; Lusk, M. T.; van Duin, A. C. T.; Goddard, W. A., III. Mechanical properties of connected carbon nanorings via molecular dynamics simulation. *Phys. Rev. B* **2005**, *72*, 085416.

[75] Çağin, T.; Gao, G.; Goddard III, W. A. Computational studies on mechanical properties of carbon nanotori. *Turk. J. Phys.* **2006**, *30*, 221–229.

[76] Feng, C.; Liew, K. M. A molecular mechanics analysis of the buckling behavior of carbon nanorings under tension. *Carbon* **2009**, *47*, 3508–3514.

[77] Feng, C.; Liew, K. M. Buckling behavior of armchair and zigzag carbon nanorings. *J. Comput. Theor. Nanosci.* **2010**, *7*, 2049–2053.

[78] Zheng, M.; Ke, C. Elastic deformation of carbon-nanotube nanorings. *Small* **2010**, *6*, 1647–1655.

[79] Zheng, M.; Ke, C. Mechanical deformation of carbon nanotube nano-rings on flat substrate. *J. Appl. Phys.* **2011**, *109*, 074304.

[80] Zhang, Z.; Yang, Z.; Wang, X.; Yuan, J.; Zhang, H.; Qiu, M.; Peng, J. The electronic structure of a deformed chiral carbon nanotorus. *J. Phys.: Condens. Matter* **2005**, *17*, 4111–4120.

[81] Ceulemans, A.; Chibotaru, L. F.; Bovin, S. A.; Fowler, P. W. The electronic structure of polyhex carbon tori. *J. Chem. Phys.* **2000**, *112*, 4271–4278.

[82] Liu, C. P.; Ding, J. W. Electronic structure of carbon nanotori:

The roles of curvature, hybridization, and disorder. *J. Phys.: Condens. Matter* **2006**, *18*, 4077–4084.

[83] Oh, D.-H.; Mee Park, J.; Kim, K. S. Structures and electronic properties of small carbon nanotube tori. *Phys. Rev. B* **2000**, *62*, 1600–1603.

[84] Yazgan, E.; Taşci, E.; Malcioğlu, O. B.; Erkoç, Ş. Electronic properties of carbon nanotoroidal structures. *J. Mol. Struct.: Theochem.* **2004**, *681*, 231–234.

[85] Wu, X.; Zhou, R.; Yang, J.; Zeng, X. C. Density-functional theory studies of step-kinked carbon nanotubes. *J. Phys. Chem. C* **2011**, *115*, 4235–4239.

[86] Haddon, R. C. Electronic properties of carbon toroids. *Nature* **1997**, *388*, 31–32.

[87] Rodríguez-Manzo, J. A.; López-Urías, F.; Terrones, M.; Terrones, H. Magnetism in corrugated carbon nanotori: The importance of symmetry, defects, and negative curvature. *Nano Lett.* **2004**, *4*, 2179–2183.

[88] Lin, M. F.; Chuu, D. S. Persistent currents in toroidal carbon nanotubes. *Phys. Rev. B* **1998**, *57*, 6731–6737.

[89] Latil, S.; Roche, S.; Rubio, A. Persistent currents in carbon nanotube based rings. *Phys. Rev. B* **2003**, *67*, 165420.

[90] Shyu, F. L.; Tsai, C. C.; Chang, C. P.; Chen, R. B.; Lin, M. F. Magnetoelectronic states of carbon toroids. *Carbon* **2004**, *42*, 2879–2885.

[91] Margańska, M.; Szopa, M.; Zipper, E. Aharonov–Bohm effect in carbon nanotubes and tori. *Physica Status Solidi B* **2005**, *242*, 285–290.

[92] Zhang, Z. H.; Yuan, J. H.; Qiu, M.; Peng, J. C.; Xiao, F. L. Persistent currents in carbon nanotori: Effects of structure deformations and chirality. *J. Appl. Phys.* **2006**, *99*, 104311.

[93] Tsai, C. C.; Shyu, F. L.; Chiu, C. W.; Chang, C. P.; Chen, R. B.; Lin, M. F. Magnetization of armchair carbon tori. *Phys. Rev. B* **2004**, *70*, 075411.

[94] Liu, C. P.; Chen, H. B.; Ding, J. W. Magnetic response of carbon nanotori: The importance of curvature and disorder. *J. Phys.: Condens. Matter* **2008**, *20*, 015206.

[95] Liu, C. P.; Xu, N. Magnetic response of chiral carbon nanotori: The dependence of torus radius. *Physica B* **2008**, *403*, 2884–2887.

[96] Rodríguez-Manzo, J. A.; López-Urías, F.; Terrones, M.; Terrones, H. Anomalous paramagnetism in doped carbon nanostructures. *Small* **2007**, *3*, 120–125.

[97] Hilder, T. A.; Hill, J. M. Orbiting atoms and C_{60} fullerenes inside carbon nanotori. *J. Appl. Phys.* **2007**, *101*, 064319.

[98] Lusk, M. T.; Hamm, N. *Ab initio* study of toroidal carbon nanotubes with encapsulated atomic metal loops. *Phys. Rev. B* **2007**, *76*, 125422.

[99] Chan, Y.; Cox, B. J.; Hill, J. M. Carbon nanotori as traps for atoms and ions. *Physica B* **2012**, *407*, 3479–3483.

[100] Mukherjee, B.; Maiti, P. K.; Dasgupta, C.; Sood, A. K. Single-file diffusion of water inside narrow carbon nanorings. *ACS Nano* **2010**, *4*, 985–991.

[101] Castillo-Alvarado, F. d. L.; Ortíz-López, J.; Arellano, J. S.; Cruz-Torres, A. Hydrogen atorage on beryllium-coated toroidal carbon nanostructure C_{120} modeled with density functional theory. *Adv. Sci. Technol.* **2010**, *72*, 188–195.

[102] Wang, M. S.; Peng, L. M.; Wang, J. Y.; Chen, Q. Shaping carbon nanotubes and the effects on their electrical and mechanical properties. *Adv. Funct. Mater.* **2006**, *16*, 1462–1468.

[103] Geblinger, N.; Ismach, A.; Joselevich, E. Self-organized nanotube serpentines. *Nat. Nanotechnol.* **2008**, *3*, 195–200.

[104] Yao, Y.; Dai, X.; Feng, C.; Zhang, J.; Liang, X.; Ding, L.; Choi, W.; Choi, J. Y.; Kim, J. M.; Liu, Z. Crinkling ultralong carbon nanotubes into serpentines by a controlled landing process. *Adv. Mater.* **2009**, *21*, 4158–4162.

[105] Kocabas, C.; Kang, S. J.; Ozel, T.; Shim, M.; Rogers, J. A. Improved synthesis of aligned arrays of single-walled carbon nanotubes and their implementation in thin film type transistor. *J. Phys. Chem. C* **2007**, *111*, 17879–17886.

[106] Duan, X.; Son, H.; Gao, B.; Zhang, J.; Wu, T.; Samsonidze, G. G.; Dresselhaus, M. S.; Liu, Z.; Kong, J. Resonant Raman spectroscopy of individual strained single-wall carbon nanotubes. *Nano Lett.* **2007**, *7*, 2116–2121.

[107] Gao, B.; Duan, X.; Zhang, J.; Wu, T.; Son, H.; Kong, J.; Liu, Z. Raman spectral probing of electronic transition energy E_{ii} Variation of Individual SWNTs under Torsional Strain. *Nano Lett.* **2007**, *7*, 750–753.

[108] Gao, B.; Duan, X.; Zhang, J.; Wu, G.; Dong, J.; Liu, Z. G-band variation of individual single-walled carbon nanotubes under torsional strain. *J. Phys. Chem. C* **2008**, *112*, 10789–10793.

[109] Xu, Z.; Buehler, M. J. Strain controlled thermomutability of single-walled carbon nanotubes. *Nanotechnology* **2009**, *20*, 185701.

[110] Lu, W. Quantum conductance of a helically coiled carbon nanotube. *Sci. Technol. Adv. Mater.* **2005**, *6*, 809–813.

[111] Liu, L.; Gao, J.; Guo, X.; Zhao, J. Electromechanical properties of zigzag-shaped carbon nanotubes. *Phys. Chem. Chem. Phys.* **2013**, *15*, 17134–17141.

[112] Wong, E. W.; Sheehan, P. E.; Lieber, C. M. Nanobeam mechanics: Elasticity, strength, and toughness of nanorods and nanotubes. *Science* **1997**, *277*, 1971–1975.

[113] Natsuki, T.; Endo, M. Stress simulation of carbon nanotubes in tension and compression. *Carbon* **2004**, *42*, 2147–2151.

[114] Xiao, J. R.; Gama, B. A.; Gillespie Jr., J. W. An analytical molecular structural mechanics model for the mechanical properties of carbon nanotubes. *Int. J. Solids Struct.* **2005**, *42*, 3075–3092.

[115] Tekleab, D.; Czerw, R.; Carroll, D.; Ajayan, P. Electronic structure of kinked multiwalled carbon nanotubes. *Appl. Phys. Lett.* **2000**, *76*, 3594–3596.

[116] Lu, J.-Q.; Wu, J.; Duan, W.; Liu, F.; Zhu, B.-F.; Gu, B.-L. Metal-to-semiconductor transition in squashed armchair carbon nanotubes. *Phys. Rev. Lett.* **2003**, *90*, 156601.

[117] Wu, J.; Zang, J.; Larade, B.; Guo, H.; Gong, X. G.; Liu, F. Computational design of carbon nanotube electromechanical pressure sensors. *Phys. Rev. B* **2004**, *69*, 153406.

[118] Baughman, R. H.; Cui, C.; Zakhidov, A. A.; Iqbal, Z.; Barisci, J. N.; Spinks, G. M.; Wallace, G. G.; Mazzoldi, A.; De Rossi, D.; Rinzler, A. G. Carbon nanotube actuators. *Science* **1999**, *284*, 1340–1344.

[119] Cao, J.; Wang, Q.; Dai, H. Electromechanical properties of metallic, quasimetallic, and semiconducting carbon nanotubes under stretching. *Phys. Rev. Lett.* **2003**, *90*, 157601.

[120] Srivastava, D.; Brenner, D. W.; Schall, J. D.; Ausman, K. D.; Yu, M.; Ruoff, R. S. Predictions of enhanced chemical reactivity at regions of local conformational strain on carbon nanotubes: Kinky chemistry. *J. Phys. Chem. B* **1999**, *103*, 4330–4337.

[121] Li, X.; Wang, X.; Zhang, L.; Lee, S.; Dai, H. Chemically derived, ultrasmooth graphene nanoribbon semiconductors. *Science* **2008**, *319*, 1229–1232.

[122] Jia, X.; Hofmann, M.; Meunier, V.; Sumpter, B. G.; Campos-Delgado, J.; Romo-Herrera, J. M.; Son, H.; Hsieh, Y.-P.; Reina, A.; Kong, J.; et al. Controlled formation of sharp zigzag and armchair edges in graphitic nanoribbons. *Science* **2009**, *323*, 1701–1705.

[123] Warner, J. H.; Schäffel, F.; Rümmeli, M. H.; Büchner, B. Examining the edges of multi-layer graphene sheets. *Chem. Mater.* **2009**, *21*, 2418–2421.

[124] Cai, J.; Ruffieux, P.; Jaafar, R.; Bieri, M.; Braun, T.; Blankenburg, S.; Muoth, M.; Seitsonen, A. P.; Saleh, M.; Feng, X. Atomically precise bottom-up fabrication of graphene nanoribbons. *Nature* **2010**, *466*, 470–473.

[125] Wu, X.; Zeng, X. C. Sawtooth-like graphene nanoribbon. *Nano Res.* **2008**, *1*, 40–45.

[126] Kou, L.; Tang, C.; Chen, C.; Guo, W. Hybrid W-shaped graphene nanoribbons: Distinct electronic and transport properties. *J. Appl. Phys.* **2011**, *110*, 124312.

[127] Yan, Q.; Huang, B.; Yu, J.; Zheng, F.; Zang, J.; Wu, J.; Gu, B.-L.; Liu, F.; Duan, W. Intrinsic current–voltage characteristics of graphene nanoribbon transistors and effect of edge doping. *Nano Lett.* **2007**, *7*, 1469–1473.

[128] Wang, Z. F.; Shi, Q. W.; Li, Q.; Wang, X.; Hou, J. G.; Zheng, H.; Yao, Y.; Chen, J. Z-shaped graphene nanoribbon quantum dot device. *Appl. Phys. Lett.* **2007**, *91*, 053109.

[129] Kong, D.; Randel, J. C.; Peng, H.; Cha, J. J.; Meister, S.; Lai, K.; Chen, Y.; Shen, Z.-X.; Manoharan, H. C.; Cui, Y. Topological insulator nanowires and nanoribbons. *Nano Lett.* **2009**, *10*, 329–333.

[130] Yu, D.; Lupton, E. M.; Gao, H.; Zhang, C.; Liu, F. A unified geometric rule for designing nanomagnetism in graphene. *Nano Res.* **2008**, *1*, 497–501.

[131] Wang, Z.; Jin, S.; Liu, F. Spatially separated spin carriers in spin-semiconducting graphene nanoribbons. *Phys. Rev. Lett.* **2013**, *111*, 096803.

[132] Li, Y.; Zhou, Z.; Shen, P.; Chen, Z. Electronic and magnetic properties of hybrid graphene nanoribbons with zigzag–armchair heterojunctions. *J. Phys. Chem. C* **2011**, *116*, 208–213.

[133] Huang, W.; Wang, J.-S.; Liang, G. Theoretical study on thermoelectric properties of kinked graphene nanoribbons. *Phys. Rev. B* **2011**, *84*, 045410.

[134] Zhang, H.-S.; Guo, Z.-X.; Gong, X.-G.; Cao, J.-X. Thermal conductivity of sawtooth-like graphene nanoribbons: A molecular dynamics study. *J. Appl. Phys.* **2012**, *112*, 123508.

[135] Koos, A. A.; Ehlich, R.; Horvath, Z. E.; Osvath, Z.; Gyulai, J.; Nagy, J. B.; Biro, L. P. STM and AFM investigation of coiled carbon nanotubes produced by laser evaporation of fullerene. *Mater. Sci. Eng.: C* **2003**, *23*, 275–278.

[136] Saveliev, A. V.; Merchan-Merchan, W.; Kennedy, L. A. Metal catalyzed synthesis of carbon nanostructures in an opposed flow methane oxygen flame. *Combust. Flame* **2003**, *135*, 27–33.

[137] Bai, J. B.; Hamon, A. L.; Marraud, A.; Jouffrey, B.; Zymla, V. Synthesis of SWNTs and MWNTs by a molten salt (NaCl) method. *Chem. Phys. Lett.* **2002**, *365*, 184–188.

[138] Ajayaghosh, A.; Vijayakumar, C.; Varghese, R.; George, S. J. Cholesterol-aided supramolecular control over chromophore packing: Twisted and coiled helices with distinct optical, chiroptical, and morphological features. *Angew. Chem. Int. Edit.* **2006**, *45*, 456–460.

[139] Yamamoto, T.; Fukushima, T.; Aida, T. Self-assembled nanotubes and nanocoils from ss-conjugated building blocks. In *Self-Assembled Nanomaterials II*. Toshimi, S., Ed.; Springer: Berlin, 2008; pp. 1–27.

[140] Fejes, D.; Hernádi, K. A review of the properties and CVD synthesis of coiled carbon nanotubes. *Materials* **2010**, *3*, 2618–2642.

[141] Hokushin, S.; Pan, L.; Nakayama, Y. Diameter control of carbon nanocoils by the catalyst of organic metals. *Jpn. J. Appl. Phys.* **2007**, *46*, 5383–5385.

[142] Li, D.; Pan, L.; Wu, Y.; Peng, W. The effect of changes in synthesis temperature and acetylene supply on the morphology of carbon nanocoils. *Carbon* **2012**, *50*, 2571–2580.

[143] Wen, Y.; Shen, Z. Synthesis of regular coiled carbon nanotubes by Ni-catalyzed pyrolysis of acetylene and a growth mechanism analysis. *Carbon* **2001**, *39*, 2369–2374.

[144] Bajpai, V.; Dai, L.; Ohashi, T. Large-scale synthesis of perpendicularly aligned helical carbon nanotubes. *J. Am. Chem. Soc.* **2004**, *126*, 5070–5071.

[145] Pan, L. J.; Zhang, M.; Nakayama, Y. Growth mechanism of carbon nanocoils. *J. Appl. Phys.* **2002**, *91*, 10058–10061.

[146] Zhang, X. F.; Zhang, Z. Polygonal spiral of coil-shaped carbon nanotubules. *Phys. Rev. B* **1995**, *52*, 5313–5317.

[147] Lu, M.; Li, H.-L.; Lau, K.-T. Formation and growth mechanism of dissimilar coiled carbon nanotubes by reduced-pressure catalytic chemical vapor deposition. *J. Phys. Chem. B* **2004**, *108*, 6186–6192.

[148] Bai, J. B. Growth of nanotube/nanofibre coils by CVD on an alumina substrate. *Mater. Lett.* **2003**, *57*, 2629–2633.

[149] Zhang, G. Y.; Jiang, X.; Wang, E. G. Self-assembly of carbon nanohelices: Characteristics and field electron emission properties. *Appl. Phys. Lett.* **2004**, *84*, 2646–2648.

[150] Varadan, V. K.; Xie, J. Synthesis of carbon nanocoils by microwave CVD. *Smart Mater. Struct.* **2002**, *11*, 728–734.

[151] Hyeon, T.; Han, S.; Sung, Y.-E.; Park, K.-W.; Kim, Y.-W. High-performance direct methanol fuel cell electrodes using solid-phase-synthesized carbon nanocoils. *Angew. Chem. Int. Edit.* **2003**, *42*, 4352–4356.

[152] Park, K.-W.; Sung, Y.-E.; Han, S.; Yun, Y.; Hyeon, T. Origin of the enhanced catalytic activity of carbon nanocoil-supported PtRu alloy electrocatalysts. *J. Phys. Chem. B* **2004**, *108*, 939–944.

[153] Kuzuya, C.; In‐Hwang, W.; Hirako, S.; Hishikawa, Y.; Motojima, S. Preparation, morphology, and growth mechanism of carbon nanocoils. *Chem. Vapor Depos.* **2002**, *8*, 57–62.

[154] Fonseca, A.; Hernadi, K.; Nagy, J. B.; Lambin, P.; Lucas, A. A. Growth mechanism of coiled carbon nanotubes. *Synthetic Met.* **1996**, *77*, 235–242.

[155] Chen, X.; Yang, S.; Takeuchi, K.; Hashishin, T.; Iwanaga, H.; Motojiima, S. Conformation and growth mechanism of the carbon nanocoils with twisting form in comparison with that of carbon microcoils. *Diam. Relat. Mater.* **2003**, *12*, 1836–1840.

[156] Bandaru, P. R.; Daraio, C.; Yang, K.; Rao, A. M. A plausible mechanism for the evolution of helical forms in nanostructure growth. *J. Appl. Phys.* **2007**, *101*, 094307.

[157] Dunlap, B. I. Relating carbon tubules. *Phys. Rev. B* **1994**, *49*, 5643–5651.

[158] Fonseca, A.; Hernadi, K.; Nagy, J. B.; Lambin, P.; Lucas, A. A. Model structure of perfectly graphitizable coiled carbon nanotubes. *Carbon* **1995**, *33*, 1759–1775.

[159] Ihara, S.; Itoh, S.; Kitakami, J.-I. Helically coiled cage forms of graphitic carbon. *Phys. Rev. B* **1993**, *48*, 5643–5647.

[160] Setton, R.; Setton, N. Carbon nanotubes: III. Toroidal structures and limits of a model for the construction of helical and S-shaped nanotubes. *Carbon* **1997**, *35*, 497–505.

[161] Akagi, K.; Tamura, R.; Tsukada, M.; Itoh, S.; Ihara, S. Electronic structure of helically coiled cage of graphitic carbon. *Phys. Rev. Lett.* **1995**, *74*, 2307–2310.

[162] Akagi, K.; Tamura, R.; Tsukada, M.; Itoh, S.; Ihara, S. Electronic structure of helically coiled carbon nanotubes: Relation between the phason lines and energy band features. *Phys. Rev. B* **1996**, *53*, 2114–2120.

[163] Biró, L. P.; Márk, G. I.; Lambin, P. Regularly coiled carbon nanotubes. *IEEE T. Nanotechnol.* **2003**, *2*, 362–367.

[164] Liu, L.; Gao, H.; Zhao, J.; Lu, J. Superelasticity of carbon nanocoils from atomistic quantum simulations. *Nanoscale Res. Lett.* **2010**, *5*, 478–483.

[165] Feng, C.; Liew, K. M. Structural stability of carbon nanosprings. *Carbon* **2011**, *49*, 4688–4694.

[166] Zhong-can, O.-Y.; Su, Z.-B.; Wang, C.-L. Coil formation in multishell carbon nanotubes: Competition between curvature elasticity and interlayer adhesion. *Phys. Rev. Lett.* **1997**, *78*, 4055–4058.

[167] Wu, J.; He, J.; Odegard, G. M.; Nagao, S.; Zheng, Q.; Zhang, Z. Giant stretchability and reversibility of tightly wound helical carbon nanotubes. *J. Am. Chem. Soc.* **2013**, *135*, 13775–13785.

[168] Volodin, A.; Ahlskog, M.; Seynaeve, E.; Van Haesendonck, C.; Fonseca, A.; Nagy, J. B. Imaging the elastic properties of coiled carbon nanotubes with atomic force microscopy. *Phys. Rev. Lett.* **2000**, *84*, 3342–3345.

[169] Hayashida, T.; Pan, L.; Nakayama, Y. Mechanical and electrical properties of carbon tubule nanocoils. *Physica B* **2002**, *323*, 352–353.

[170] Chen, X.; Zhang, S.; Dikin, D. A.; Ding, W.; Ruoff, R. S.; Pan, L.; Nakayama, Y. Mechanics of a carbon nanocoil. *Nano Lett.* **2003**, *3*, 1299–1304.

[171] Huang, W. M. Mechanics of coiled nanotubes in uniaxial tension. *Mater. Sci. Eng.: A* **2005**, *408*, 136–140.

[172] Neng-Kai, C.; Shuo-Hung, C. Determining mechanical properties of carbon microcoils using lateral force microscopy. *IEEE T. Nanotechnol.* **2008**, *7*, 197–201.

[173] Poggi, M. A.; Boyles, J. S.; Bottomley, L. A.; McFarland, A. W.; Colton, J. S.; Nguyen, C. V.; Stevens, R. M.; Lillehei, P. T. Measuring the compression of a carbon nanospring. *Nano Lett.* **2004**, *4*, 1009–1016.

[174] Fonseca, A. F. D.; Galvao, D. S. Mechanical properties of nanosprings. *Phys. Rev. Lett.* **2004**, *92*, 175502.

[175] da Fonseca, A. F.; Malta, C. P.; Galvao, D. S. Mechanical properties of amorphous nanosprings. *Nanotechnology* **2006**, *17*, 5620–5626.

[176] Ghaderi, S. H.; Hajiesmaili, E. Nonlinear analysis of coiled carbon nanotubes using molecular dynamics finite element method. *Mater. Sci. Eng.: A* **2013**, *582*, 225–234.

[177] Ghaderi, S. H.; Hajiesmaili, E. Molecular structural mechanics applied to coiled carbon nanotubes. *Comput. Mater. Sci.* **2010**, *55*, 344–349.

[178] Coluci, V. R.; Fonseca, A. F.; Galvão, D. S.; Daraio, C. Entanglement and the nonlinear elastic behavior of forests of coiled carbon nanotubes. *Phys. Rev. Lett.* **2008**, *100*, 086807.

[179] Kaneto, K.; Tsuruta, M.; Motojima, S. Electrical properties of carbon micro coils. *Synthetic Met.* **1999**, *103*, 2578–2579.

[180] Shen, J.; Chen, Z.; Wang, N.; Li, W.; Chen, L. Electrical properties of a single microcoiled carbon fiber. *Appl. Phys. Lett.* **2006**, *89*, 153132.

[181] Fujii, M.; Matsui, M.; Motojima, S.; Hishikawa, Y. Magnetoresistance in carbon micro-coils obtained by chemical vapor deposition. *Thin Solid Film.* **2002**, *409*, 78–81.

[182] Ebbesen, T. W.; Lezec, H. J.; Hiura, H.; Bennett, J. W.; Ghaemi, H. F.; Thio, T. Electrical conductivity of individual carbon nanotubes. *Nature* **1996**, *382*, 54–56.

[183] Chiu, H.-S.; Lin, P.-I.; Wu, H.-C.; Hsieh, W.-H.; Chen, C.-D.; Chen, Y.-T. Electron hopping conduction in highly disordered carbon coils. *Carbon* **2009**, *47*, 1761–1769.

[184] Tang, N.; Kuo, W.; Jeng, C.; Wang, L.; Lin, K.; Du, Y. Coil-in-coil carbon nanocoils: 11 gram-scale synthesis, single nanocoil electrical properties, and electrical contact improvement. *ACS Nano* **2010**, *4*, 781–788.

[185] Liu, L.; Gao, H.; Zhao, J.; Lu, J. Quantum conductance of armchair carbon nanocoils: Roles of geometry effects. *Sci. China Phys. Mech. Astron.* **2011**, *54*, 841–845.

[186] Liu, J.; Webster, S.; Carroll, D. L. Highly aligned coiled nitrogen-doped carbon nanotubes synthesized by injection-assisted chemical vapor deposition. *Appl. Phys. Lett.* **2006**, *88*, 213119.

[187] Jafri, R. I.; Rajalakshmi, N.; Ramaprabhu, S. Nitrogen-doped multi-walled carbon nanocoils as catalyst support for oxygen reduction reaction in proton exchange membrane fuel cell. *J. Power Sources* **2010**, *195*, 8080–8083.

[188] Wen, J.; Zhang, Y.; Tang, N.; Wan, X.; Xiong, Z.; Zhong, W.; Wang, Z.; Wu, X.; Du, Y. Synthesis, photoluminescence, and magnetic properties of nitrogen-doping helical carbon nanotubes. *J. Phys. Chem. C* **2011**, *115*, 12329–12334.

[189] Rakhi, R. B.; Chen, W.; Alshareef, H. N. Conducting polymer/carbon nanocoil composite electrodes for efficient supercapacitors. *J. Mater. Chem.* **2012**, *22*, 5177–5183.

[190] Saito, Y.; Uemura, S.; Hamaguchi, K. Cathode ray tube lighting elements with carbon nanotube field emitters. *Jpn. J. Appl. Phys.* **1998**, *37*, L346–L348.

[191] Choi, W. B.; Chung, D. S.; Kang, J. H.; Kim, H. Y.; Jin, Y. W.; Han, I. T.; Lee, Y. H.; Jung, J. E.; Lee, N. S.; Park, G. S. Fully sealed, high-brightness carbon-nanotube field-emission display. *Appl. Phys. Lett.* **1999**, *75*, 3129–3131.

[192] Jiao, J.; Einarsson, E.; Tuggle, D. W.; Love, L.; Prado, J.; Coia, G. M. High-yield synthesis of carbon coils on tungsten substrates and their behavior in the presence of an electric field. *J. Mater. Res.* **2003**, *18*, 2580–2587.

[193] Einarsson, E.; Tuggle, D. W.; Jiao, J. *In situ* alignment of carbon nanocoils and their field emission behavior induced by an electric field. *Appl. Phys. A* **2004**, *79*, 2049–2054.

[194] Hokushin, S.; Pan, L.; Konishi, Y.; Tanaka, H.; Nakayama, Y. Field emission properties and structural changes of a stand-alone carbon nanocoil. *Jpn. J. Appl. Phys.* **2007**, *46*, L565–L567.

[195] Ok, J. G.; Kim, B. H.; Sung, W. Y.; Lee, S. M.; Lee, S. W.; Kim, W. J.; Park, J. W.; Chu, C. N.; Kim, Y. H. Electrical discharge machining of carbon nanomaterials in air: Machining characteristics and the advanced field emission applications. *J. Micromech. Microeng.* **2008**, *18*, 025007.

[196] Lahiri, I.; Seelaboyina, R.; Hwang, J. Y.; Banerjee, R.; Choi, W. Enhanced field emission from multi-walled carbon nanotubes grown on pure copper substrate. *Carbon* **2010**, *48*, 1531–1538.

[197] Tang, N.; Yang, Y.; Lin, K.; Zhong, W.; Au, C.; Du, Y. Synthesis of plait-like carbon nanocoils in ultrahigh yield, and their microwave absorption properties. *J. Phys. Chem. C* **2008,** *112*, 10061–10067.

[198] Liu, Z.; Bai, G.; Huang, Y.; Li, F.; Ma, Y.; Guo, T.; He, X.; Lin, X.; Gao, H.; Chen, Y. Microwave absorption of single-walled carbon nanotubes/soluble cross-linked polyurethane composites. *J. Phys. Chem. C* **2007**, *111*, 13696–13700.

[199] Tang, N.; Zhong, W.; Au, C.; Yang, Y.; Han, M.; Lin, K.; Du, Y. Synthesis, microwave electromagnetic, and micro-wave absorption properties of twin carbon nanocoils. *J. Phys. Chem. C* **2008**, *112*, 19316–19323.

[200] Gupta, B. K.; Shanker, V.; Arora, M.; Haranath, D. Photoluminescence and electron paramagnetic resonance studies of springlike carbon nanofibers. *Appl. Phys. Lett.* **2009**, *95*, 073115.

[201] Ma, H.; Pan, L.; Zhao, Q.; Zhao, Z.; Zhao, J.; Qiu, J. Electrically driven light emission from a single suspended carbon nanocoil. *Carbon* **2012**, *50*, 5537–5542.

[202] Ma, H.; Pan, L.; Zhao, Q.; Peng, W. Near-infrared response of a single carbon nanocoil. *Nanoscale* **2013**, *5*, 1153–1158.

[203] Motojima, S.; Chen, X.; Yang, S.; Hasegawa, M. Properties

[204] Volodin, A.; Buntinx, D.; Ahlskog, M.; Fonseca, A.; Nagy, J. B.; Van Haesendonck, C. Coiled carbon nanotubes as self-sensing mechanical resonators. *Nano Lett.* **2004**, *4*, 1775–1779.

[205] Bell, D. J.; Sun, Y.; Zhang, L.; Dong, L. X.; Nelson, B. J.; Grutzmacher, D. Three-dimensional nanosprings for electromechanical sensors. *Sensor. Actuat. A: Phys.* **2006**, *130–131*, 54–61.

[206] Kato, Y.; Adachi, N.; Okuda, T.; Yoshida, T.; Motojima, S.; Tsuda, T. Evaluation of induced electromotive force of a carbon micro coil. *Jpn. J. Appl. Phys.* **2003**, *42*, 5035–5037.

[207] Shaoming, Y.; Xiuqin, C.; Aoki, H.; Motojima, S. Tactile microsensor elements prepared from aligned superelastic carbon microcoils and polysilicone matrix. *Smart Mater. Struct.* **2006**, *15*, 687–694.

[208] Greenshields, M. W. C. C.; Hümmelgen, I. A.; Mamo, M. A.; Shaikjee, A.; Mhlanga, S. D.; van Otterlo, W. A. L.; Coville, N. J. Composites of polyvinyl alcohol and carbon (coils, undoped and nitrogen doped multiwalled carbon nanotubes) as ethanol, methanol and toluene vapor sensors. *J. Nanosci. Nanotechnol.* **2011**, *11*, 10211–10218.

[209] Lau, K.-T.; Lu, M.; Liao, K. Improved mechanical properties of coiled carbon nanotubes reinforced epoxy nanocomposites. *Compos. Part A: Appl. Sci. Manuf.* **2006**, *37*, 1837–1840.

[210] Yoshimura, K.; Nakano, K.; Miyake, T.; Hishikawa, Y.; Motojima, S. Effectiveness of carbon microcoils as a reinforcing material for a polymer matrix. *Carbon* **2006**, *44*, 2833–2838.

[211] Li, X.-F.; Lau, K.-T.; Yin, Y.-S. Mechanical properties of epoxy-based composites using coiled carbon nanotubes. *Compos. Part A: Appl. Sci. Manuf.* **2006**, *37*, 1837–1840.

[212] Sanada, K.; Takada, Y.; Yamamoto, S.; Shindo, Y. Analytical and experimental characterization of stiffness and damping in carbon nanocoil reinforced polymer composites. *J. Solid Mech. Mater. Eng.* **2008**, *2*, 1517–1527.

[213] Katsuno, T.; Chen, X.; Yang, S.; Motojima, S.; Homma, M.; Maeno, T.; Konyo, M. Observation and analysis of percolation behavior in carbon microcoils/silicone-rubber composite sheets. *Appl. Phys. Lett.* **2006**, *88*, 232115.

[214] Yoshimura, K.; Nakano, K.; Miyake, T.; Hishikawa, Y.; Kuzuya, C.; Katsuno, T.; Motojima, S. Effect of compressive and tensile strains on the electrical resistivity of carbon microcoil/silicone-rubber composites. *Carbon* **2007**, *45*, 1997–2003.

[215] Bi, H.; Kou, K.-C.; Ostrikov, K.; Yan, L.-K.; Wang, Z.-C. Microstructure and electromagnetic characteristics of Ni

nanoparticle film coated carbon microcoils. *J. Alloy. Compd.* **2009**, *478*, 796–800.

[216] Nakamatsu, K.; Igaki, J.; Nagase, M.; Ichihashi, T.; Matsui, S. Mechanical characteristics of tungsten-containing carbon nanosprings grown by FIB-CVD. *Microelectron. Eng.* **2006**, *83*, 808–810.

[217] Wu, X.-L.; Liu, Q.; Guo, Y.-G.; Song, W.-G. Superior storage performance of carbon nanosprings as anode materials for lithium-ion batteries. *Electrochem. Commun.* **2009**, *11*, 1468–1471.

[218] Wang, L.; Li, C.; Gu, F.; Zhang, C. Facile flame synthesis and electrochemical properties of carbon nanocoils. *J. Alloy. Compd.* **2009**, *473*, 351–355.

[219] Rakhi, R. B.; Cha, D.; Chen, W.; Alshareef, H. N. Electrochemical energy storage devices using electrodes incorporating carbon nanocoils and metal oxides nano-particles. *J. Phys. Chem. C* **2011**, *115*, 14392–14399.

[220] Ivanovskii, A. L. Non-carbon nanotubes: Synthesis and simulation. *Russ. Chem. Rev.* **2002**, *71*, 175–194.

[221] Xiong, Y.; Mayers, B. T.; Xia, Y. Some recent developments in the chemical synthesis of inorganic nanotubes. *Chem. Commun.* **2005**, 5013–5022.

[222] Tenne, R. Inorganic nanotubes and fullerene-like nano-particles. *Nat. Nanotechnol.* **2006**, *1*, 103–111.

[223] Goldberger, J.; Fan, R.; Yang, P. Inorganic nanotubes: A novel platform for nanofluidics. *Acc. Chem. Res.* **2006**, *39*, 239–248.

[224] Zeng, H.; Zhi, C.; Zhang, Z.; Wei, X.; Wang, X.; Guo, W.; Bando, Y.; Golberg, D. "White graphenes": Boron nitride nanoribbons via boron nitride nanotube unwrapping. *Nano Lett.* **2010**, *10*, 5049–5055.

[225] Radisavljevic, B.; Radenovic, A.; Brivio, J.; Giacometti, V.; Kis, A. Single-layer MoS₂ transistors. *Nat. Nanotechnol.* **2011**, *6*, 147–150.

[226] Lino, A. A.; Chacham, H. L.; Mazzoni, M. R. S. C. Edge states and half-metallicity in TiO₂ nanoribbons. *J. Phys. Chem. C* **2011**, *115*, 18047–18050.

[227] Zhang, H.; Li, X.-B.; Liu, L.-M. Tunable electronic and magnetic properties of WS₂ nanoribbons. *J. Appl. Phys.* **2013**, *114*, 093710.

[228] Biswas, S.; Kar, S.; Ghoshal, T.; Ashok, V. D.; Chakrabarti, S.; Chaudhuri, S. Fabrication of GaN nanowires and nanoribbons by a catalyst assisted vapor–liquid–solid process. *Mater. Res. Bull.* **2007**, *42*, 428–436.

[229] Camacho-Bragado, G. A.; Jose-Yacaman, M. Self-assembly of molybdite nanoribbons. *Appl. Phys. A* **2006**, *82*, 19–22.

[230] Cao, X. B.; Xie, Y.; Zhang, S. Y.; Li, F. Q. Ultra-thin trigonal selenium nanoribbons developed from series-wound beads. *Adv. Mater.* **2004**, *16*, 649–653.

[231] Jin, C.; Lin, F.; Suenaga, K.; Iijima, S. Fabrication of a freestanding boron nitride single layer and its defect assignments. *Phys. Rev. Lett.* **2009**, *102*, 195505.

[232] Zhi, C.; Bando, Y.; Tang, C.; Kuwahara, H.; Golberg, D. Large-scale fabrication of boron nitride nanosheets and their utilization in polymeric composites with improved thermal and mechanical properties. *Adv. Mater.* **2009**, *21*, 2889–2893.

[233] Ataca, C.; Sahin, H.; Ciraci, S. Stable, single-layer MX₂ transition-metal oxides and dichalcogenides in a honeycomb-like structure. *J. Phys. Chem. C* **2012**, *116*, 8983–8999.

[234] Ma, Y.; Dai, Y.; Guo, M.; Niu, C.; Lu, J.; Huang, B. Electronic and magnetic properties of perfect, vacancy-doped, and nonmetal adsorbed MoSe₂, MoTe₂ and WS₂ monolayers. *Phys. Chem. Chem. Phys.* **2011**, *13*, 15546–15553.

[235] Lee, Y.-H.; Yu, L.; Wang, H.; Fang, W.; Ling, X.; Shi, Y.; Lin, C.-T.; Huang, J.-K.; Chang, M.-T.; Chang, C.-S. Synthesis and transfer of single-layer transition metal disulfides on diverse surfaces. *Nano Lett.* **2013**, *13*, 1852–1857.

[236] Aufray, B.; Kara, A.; Vizzini, S.; Oughaddou, H.; Léandri, C.; Ealet, B.; Le Lay, G. Graphene-like silicon nanoribbons on Ag (110): A possible formation of silicene. *Appl. Phys. Lett.* **2010**, *96*, 183102.

[237] De Padova, P.; Quaresima, C.; Ottaviani, C.; Sheverdyaeva, P. M.; Moras, P.; Carbone, C.; Topwal, D.; Olivieri, B.; Kara, A.; Oughaddou, H. Evidence of graphene-like electronic signature in silicene nanoribbons. *Appl. Phys. Lett.* **2010**, *96*, 261905.

[238] Feng, B.; Ding, Z.; Meng, S.; Yao, Y.; He, X.; Cheng, P.; Chen, L.; Wu, K. Evidence of silicene in honeycomb structures of silicon on Ag (111). *Nano Lett.* **2012**, *12*, 3507–3511.

[239] Gao, J.; Zhao, J. Initial geometries, interaction mechanism and high stability of silicene on Ag (111) surface. *Sci. Rep.* **2012**, *2*, 861–868.

[240] Liu, H.; Gao, J.; Zhao, J. Silicene on substrates: A way to preserve or tune its electronic properties. *J. Phys. Chem. C* **2013**, *117*, 10353–10359.

[241] Gao, J.; Zhang, J.; Liu, H.; Zhang, Q.; Zhao, J. Structures, mobilities, electronic and magnetic properties of point defects in silicene. *Nanoscale* **2013**, *5*, 9785–9792.

[242] Wang, Z.; Su, N.; Liu, F. Prediction of a two-dimensional organic topological insulator. *Nano Lett.* **2013**, *13*, 2842–2845.

[243] Liu, Z.; Wang, Z.-F.; Mei, J.-W.; Wu, Y.-S.; Liu, F. Flat Chern band in a two-dimensional organometallic framework. *Phys. Rev. Lett.* **2013**, *110*, 106804.

[244] Wang, Z. F.; Liu, Z.; Liu, F. Quantum anomalous Hall effect in 2D organic topological insulators. *Phys. Rev. Lett.* **2013**, *110*, 196801.

[245] Wang, Z. F.; Liu, Z.; Liu, F. Organic topological insulators in organometallic lattices. *Nat. Commun.* **2013**, *4*, 1471–1475.

[246] Golberg, D.; Bando, Y.; Bourgeois, L.; Kurashima, K.; Sato, T. Insights into the structure of BN nanotubes. *Appl. Phys. Lett.* **2000**, *77*, 1979–1981.

[247] Golberg, D.; Costa, P. M. F. J.; Lourie, O.; Mitome, M.; Bai, X.; Kurashima, K.; Zhi, C.; Tang, C.; Bando, Y. Direct force measurements and kinking under elastic deformation of individual multiwalled boron nitride nanotubes. *Nano Lett.* **2007**, *7*, 2146–2151.

[248] Tian, B.; Xie, P.; Kempa, T. J.; Bell, D. C.; Lieber, C. M. Single-crystalline kinked semiconductor nanowire superstructures. *Nat. Nanotechnol.* **2009**, *4*, 824–829.

[249] Su, L.; Xiaozhong, Z.; Lihuan, Z.; Min, G. Twinning-induced kinking of Sb-doped ZnO nanowires. *Nanotechnology* **2010**, *21*, 435602.

[250] Pevzner, A.; Engel, Y.; Elnathan, R.; Tsukernik, A.; Barkay, Z.; Patolsky, F. Confinement-guided shaping of semiconductor nanowires and nanoribbons: "Writing with nanowires". *Nano Lett.* **2012**, *12*, 7–12.

[251] Liu, B.; Bando, Y.; Liu, L.; Zhao, J.; Masanori, M.; Jiang, X.; Golberg, D. Solid–solution semiconductor nanowires in pseudobinary systems. *Nano Lett.* **2013**, *13*, 85–90.

[252] Terauchi, M.; Tanaka, M.; Matsuda, H.; Takeda, M.; Kimura, K. Helical nanotubes of hexagonal boron nitride. *J. Electron Microsc.* **1997**, *46*, 75–78.

[253] Gao, P. X.; Mai, W.; Wang, Z. L. Superelasticity and nanofracture mechanics of ZnO nanohelices. *Nano Lett.* **2006**, *6*, 2536–2543.

[254] Jung, J. H.; Yoshida, K.; Shimizu, T. Creation of novel double-helical silica nanotubes using binary gel system. *Langmuir* **2002**, *18*, 8724–8727.